1. Report No. UI-23-RP-01	2. Government Accession No N/A	3. Recipient's Catalog No. N/A
4. Title and Subtitle Shape Memory Alloy Transverse Reinforcement for Solving End Region Problems in Precast Bridge Girders End Regions		5. Report Date February, 2026
		6. Performing Organization Code N/A

7. Author(s) Bassem Andrawes, Ph.D., P.E., F.ASCE, (https://orcid.org/0000-0002-8954-3751) Siyoung Park, (https://orcid.org/0000-0003-2350-4079)	8. Performing Organization Report No. UI-23-RP-01

9. Performing Organization Name and Address University of Illinois Urbana-Champaign 205 North Mathews Ave. Urbana, IL 61801-2352	10. Work Unit No. N/A
	11. Contract or Grant No. 69A3552348333

12. Sponsoring Organization Name and Address Transportation Infrastructure Precast Innovation Center (TRANS-IPIC) University of Illinois Urbana-Champaign. Civil & Environmental Engineering. 205 N Mathews Ave, Urbana, IL 61801 US Department of Transportation Office of Research, Development and Technology (RD&T) 1200 New Jersey Avenue, SE Washington, DC 201590	13. Type of Report and Period Covered Final Report August, 2023 – December, 2025
	14. Sponsoring Agency Code N/A

15. Supplementary Notes

For additional reports and information, visit the TRANS-IPIC website https://trans-ipic.illinois.edu

16. Abstract
This project introduces an innovative method that utilizes shape memory alloys (SMAs), a new class of smart materials, as transverse reinforcement in the end regions of precast prestressed concrete (PC) bridge girders. The proposed solution effectively addresses the long-standing issue of damage in the end regions of PC bridge girders caused by the application of prestressing force. SMA transverse reinforcement, known for its shape recovery capability, can help prevent cracking in these critical areas while reducing the congestion of steel reinforcement typically found in highly reinforced sections of bridge girders. The project involved both numerical and experimental studies to investigate damage mitigation during the release of prestress in PC girders. This was achieved by placing transverse SMA bars within the concrete at the end regions of the girders and generating the prestressing force through SMA activation. The results validate the effectiveness of this new reinforcement method in reducing and healing damage in the end regions of PC bridge girders.

17. Key Words Bridge girders, concrete, splitting cracks, bursting stress, shape memory alloy, recovery stress, prestress force, transverse reinforcement, end region	18. Distribution Statement No restrictions.		
19. Security Classification (of this report) Unclassified.	20. Security Classification (of this page) Unclassified.	21. No. of Pages 42	22. Price N/A

Transportation Infrastructure Precast Innovation Center (TRANS-IPIC)

University Transportation Center (UTC)

Shape Memory Alloy Transverse Reinforcement for Solving End Region Problems in Precast Bridge Girders End Regions

Project No.: UI-23-RP-01

FINAL REPORT

Submitted by:
Bassem Andrawes (PI), Ph.D., P.E., F.ASCE (andrawes@illinois.edu)
Proferssor
Department of Civil and Environmental Engineering
University of Illinois at Urbana-Champaign

Siyoung Park
Graduate Research Assistant
Department of Civil and Environmental Engineering
University of Illinois at Urbana-Champaign

Submitted to:
TRANS-IPIC UTC
University of Illinois Urbana-Champaign
Urbana, IL

Executive Summary:

This project report evaluates the effect of shape memory alloy (SMA) reinforcement as a transverse reinforcement in precast concrete (PC) bridge girders using finite element (FE) analysis and experimental studies.

In the FE analysis, a preliminary study of a bridge girder model with a Bulb-Tee (BT) section was conducted to evaluate end region damage resulting from prestress release. Stirrups in the end region were partially replaced with SMA stirrups to prove the effectiveness of SMA's prestressing force in mitigating splitting cracks propagated by de-tensioning of prestress. By using the tensile damage index, crack area, and crack width as parameters to assess damage in the end region, the SMA stirrup was effective in reducing cracks and improving serviceability (durability) in the end region of girders.

FE analysis was also performed to simulate the designed experimental specimens. The experimental results of SMA activation were modeled using FE modeling to synchronize the results. For future studies, diverse variables (including SMA bar shape, interfacial bonding, and reinforcement placement) were designed and analyzed using replicated models.

Precast prestressed concrete girders were prepared to test the prestressing effect by transverse SMA reinforcement in the end region and to examine the prestressing force's effectiveness in mitigating splitting damage. A distinct test setup was constructed to simulate prestress transfer without requiring a long specimen for the prestress transfer length. First, the prestressing effect of SMA activation was examined under a fixed-specimen condition. Then, an excessive load was applied to the girder flange to induce splitting cracks in the web. Specimens with steel stirrup-only and SMA stirrup-replaced models were experimented with in the test setup. Visual inspection and strain values were used to evaluate the effect of the SMA stirrup.

The behavior of the bent SMA bar was also investigated to understand the effect of SMA detailing during activation and to utilize the SMA bar as transverse reinforcement in the end region of precast prestressed girders. Experimental and numerical studies delved into the opening effect of the SMA bar and its impact on the surrounding concrete.

In conclusion, SMA bars were utilized as transverse reinforcement in the end regions of precast prestressed girders. This project aimed to introduce prestressing forces in the vertical direction at the end region to mitigate damage and reduce crack propagation.

Table of Contents

1. Problem description:

Despite the success of the concrete prestressing technology in the longitudinal direction, it has not been implemented in the transverse direction (i.e., prestressed stirrups, spirals, etc.) due to many practical challenges. The reason is simple; no practical method exists for prestressing internal shear reinforcement, such as hoops, stirrups, or spirals, because these reinforcements are fully embedded in the concrete; hence, gripping the reinforcement ends for prestressing is not feasible. This research investigated a new method for applying prestressing in the transverse direction using a class of metallic materials known as shape memory alloys (SMAs). The use of prestressed transverse reinforcement in precast/prestressed members could significantly impact how prestressed concrete (PC) members are designed. For example, it will potentially impact the shear strength and provide better crack control, help with reducing significantly bursting and splitting stresses at end regions, reduce the size of members, and improve steel bond strength with concrete, which will, in turn, minimize transfer/development lengths, enable early release of strands, eliminate steel congestion, especially at end regions, enhance the constructability of joint connections with lap splices, etc. This research aligns with the mission of TRANS-IPIC to improve the durability of PC transportation infrastructure and extend its service life. It aligns with the US Department of Transportation's (USDOT's) strategic goal of performing transformative research that will advance the transportation infrastructure by introducing a novel reinforcement type that can innovatively mitigate PC infrastructure damage.

2. Background:
2.1 End Region Splitting Cracks Due to Prestress Transfer

The end regions of PC members are often subjected to cracking when high prestressing forces are transferred during the de-tensioning of the strands. The tensile stresses that cause cracking at the end regions could be categorized as bursting and spalling stresses (Iyengar and Prabhakara 1971; Marshall and Mattock 1962; O'Callaghan and Bayrak 2007). Studies have shown that bursting stresses occur along the strand direction when highly centered prestressing loads at the anchorage zone spread out in S-shaped curves (**Fig. 1(a)**) (Dunkman 2009; Fenwick and Lee 1986; Shin and Yu 2018). The load distribution within the transfer zone of pretensioned members results in tensile bursting stresses and propagating cracks. In addition, the radial stresses generated from the expansion of prestressing strands during prestress transfer add up to the bursting stresses. Spalling stress is more closely related to the geometry of the members (Fenwick and Lee 1986; Sarles and Itani 1984; Steensels et al. 2019). Spalling stress occurs either because of the convex shape of the surface after applying excessive prestressing force or the high eccentricity of the strands with respect to the centroidal axis of the prestressed beam. As illustrated in **Fig. 1(b)**, high compressive forces applied to the flanges are distributed throughout the entire depth of the beam section, applying bending stresses at the mid-height regions. Especially with deep bulb-tee or I girders, excessive tensile stress is expected at the web region, which can trigger splitting cracks.

Several early studies were focused on overcoming the cracking at the end region of PC members during prestress transfer (Breen 1994; Gergely and Sozen 1967; Marshall and Mattock 1962). Marshall and Mattock (1962) measured the strain at the stirrups in end regions during prestress transfer to relate it to concrete cracking. They conducted several experiments to define the relationship between the applied prestressing force and the required cross-sectional area of the steel bar. Gergely and Sozen (1967) evaluated the bending moment applied at the end region and determined the tensile forces acting on the transverse rebars. Their analysis used the equilibrium method, simplifying the estimation of rebar requirements. These studies were summarized and adapted to specifications, such as the American Association of State Highway and Transportation Officials (AASHTO) Load and Resistance Factor Design (LRFD) Specifications (AASHTO 2024). In addition, design guidelines such as the Precast Concrete Institute (PCI) design manual (PCI 2023) were published for basic designs of PC members. More

recently, PC members with larger dimensions (i.e., Bulb-Tee (BT)-72 and BT-78) and larger diameter strands (i.e., 0.6 in.) are utilized in structures (Geren and Tadros 1994; O'Callaghan and Bayrak 2007; Ronanki et al. 2017; Ross et al. 2014). The increasing size of the sections and the prestressing strands applied more excessive tensile forces to the end region, causing cracking problems. To mitigate end region splitting cracking at PC members during prestress transfer, SMA bars will be investigated for use as transverse reinforcement in the end regions.
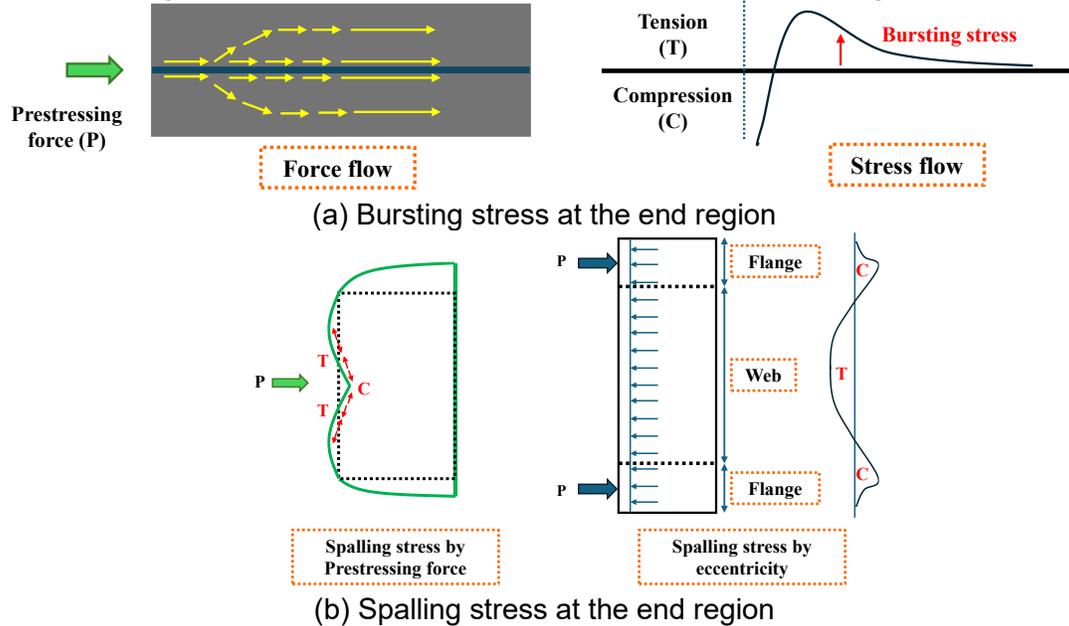
(a) Bursting stress at the end region

(b) Spalling stress at the end region

Fig. 1 Tensile stress induced by prestress transfer

2.2 Background on Shape Memory Alloy

Shape memory alloys (SMAs) are a group of metallic alloys that exhibit unique characteristics known as the shape memory effect (SME). **Fig. 2** shows the thermal hysteresis of SMA in different microstructural phases. In the martensite phase, SMA deforms by loading and unloading. The SMA atoms lie in the de-twinned martensite phase in a deformed shape and transform to the austenite phase upon heating beyond the austenite start temperature (T_{As}), fully transforming after passing the austenite finish temperature (T_{Af}). This phase transformation is also referred to as "Activation". SME is associated with recovering the SMA's original shape after experiencing deformation beyond the elastic limit during the activation period.

Researchers have investigated the use of SMA's SME in prestressing applications. Embedding elongated SMA reinforcement (bars or wires) in the concrete and activating (heating) it will generate internal compressive prestress in the concrete; thanks to the movement constraint provided by the concrete, which inhibits the SMA reinforcement from shrinking back to its original length (**Fig. 2(d)**). The prestressing effect was studied in applications such as concrete column confinement (Chen and Andrawes 2017; Jung et al. 2018; Suhail et al. 2020), flexural and shear capacity strengthening (Ghafoori et al. 2019; Zhao and Andrawes 2020), and local zone prestressing (Sung and Andrawes 2024; Zhao and Andrawes 2020). In most published works, small-diameter SMA wires were applied outside the concrete to easily induce activation for building prestressing forces. More recently, studies on heating the SMA inside concrete have been explored, making it possible to use it as an internal prestressing source.

NiTi-based alloys are among the most studied and commercially available alloys. Among diverse NiTi-based alloys, SMAs with a wide thermal hysteresis, i.e., large phase transformation temperature range, are the most suitable for structural prestressing applications. NiTiNb is one of

the Ni-based SMAs that are known for their wide thermal hysteresis (Dagdelen et al. 2020; Jiang et al. 2016; Pan et al. 2023).

Several researchers investigated the application of NiTiNb wires and bars for shape memory effect in structures (Chen and Andrawes 2017; Choi et al. 2011; Dommer and Andrawes 2012; Park and Andrawes 2025; Pérez-Claros and Andrawes 2025; Sherif et al. 2014; Shin and Andrawes 2010; Suhail et al. 2020; Sung and Andrawes 2024). Studies showed that NiTiNb wire with a diameter of 0.08 in. can build a recovery stress over 70 ksi by activation and maintain the stress level in cold (-10°C) and room temperature (Dommer and Andrawes 2012). More recently, a larger NiTiNb bar with a diameter of 0.24 in. has been investigated (Andrawes et al. 2024). They showed that the large-diameter SMA bar, more suitable for structural applications, developed a recovery stress of 40 ksi.
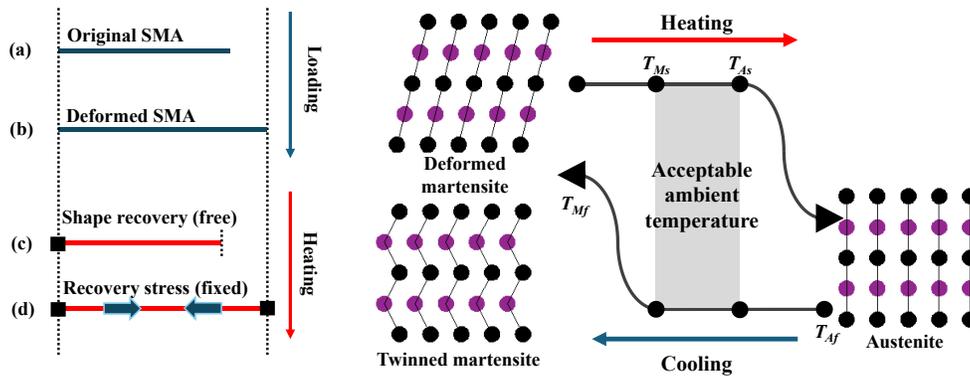

Fig. 2 Thermal hysteresis of SMA

3. Research scope and objectives:

This research project aims to investigate the use of a new material, the shape memory alloy (SMA), as the primary transverse prestressing reinforcement in the end region of precast prestressed girders to mitigate various forms of structural damage, including splitting cracks and sustained serviceability deterioration. The concept of using SMA as transverse reinforcement is studied in three primary directions. The first direction of the project (**Task 1**) focuses on designing the specimens using the finite element (FE) method. The behavior of specimens is evaluated through a detailed FE analysis. The research determines the effectiveness of SMA transverse reinforcement in mitigating splitting cracks by comparing non-prestressed and prestressed models at the end region. The second research direction (**Task 2**) focuses on fabricating, instrumenting, and testing laboratory specimens. Several small-scale specimens and large-scale beam girder specimens are manufactured and tested. The specimens provide the opportunity to examine different end regions with various designs, detailing, and SMA heating (activation) methods. The third project direction (**Task 3**) investigates SMA activation methods. Electrical resistivity and electromagnetic induction heating methods are explored to heat the SMA within concrete. Along with activating the SMA, the impact of SMA heating on the surrounding concrete and SMA's behavior are investigated to enable its effective use within the concrete as a primary transverse reinforcement.

4. Research description:
4.1 Finite element (FE) analysis on BT-72 precast prestressed girder
The finite element (FE) method was employed to numerically evaluate the effectiveness of SMA (NiTiNb) stirrups at the end region of precast prestressed girders to mitigate splitting cracks during prestress transfer. The study concept was first examined by evaluating end-region damage to the BT-72 girder caused by prestress transfer. **Fig. 3** shows the details of the BT-72 model. The girder

model was designed based on the PCI Bridge Design Manual (PCI 2023) and the AASHTO LRFD (AASHTO 2024) guidelines. Four types of models with the same geometry were designed, but the end region stirrups' layout and type were modified as shown in **Fig.3(c)**. The length of the girder model was designed to be 120 ft, being symmetric about the centerline. Prestressing strands were designed to be stressed up to 75% of their ultimate strength (202.5 ksi) by placing thirty-six straight strands at the bottom flange and twelve draped strands at the top flange with 2 in. spacing. The double-legged No. 5 stirrups at 4 in. spacing and No. 4 confinement reinforcement at 6 in. spacing were designed to reinforce the end region to prevent end region splitting cracks. The end region of the BT-72 girder was defined as extending up to one-quarter of the girder height (18 in.), where five stirrups are placed in the control specimen (**Fig. 3(c)**). To evaluate the effectiveness of SMA stirrups, three cases were designed, in which the number of end stirrups is 3 or 5, and the number of SMA stirrups is 1 or 2. Numerical models were labeled as "BT-72", "5S1", "5S2", and "3S1", where "BT-72" is the control specimen, and others were labeled in the sequence of the number of end stirrups and the number of SMA stirrups.
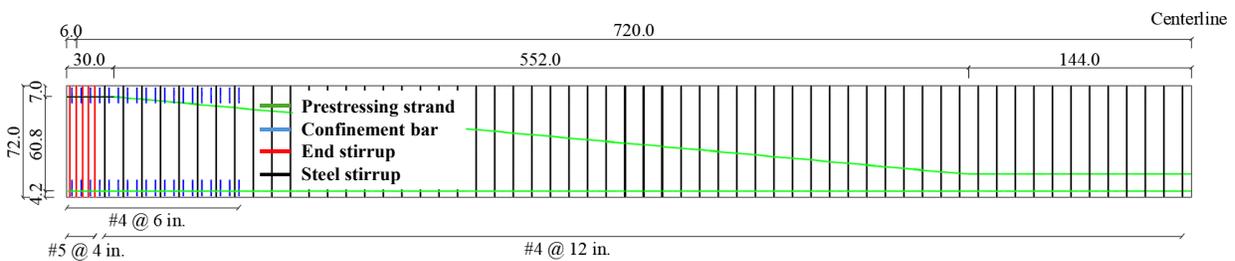
(a) Front view of BT-72 model (unit: in.)
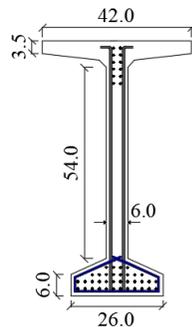
(b) Section view of BT-72 model
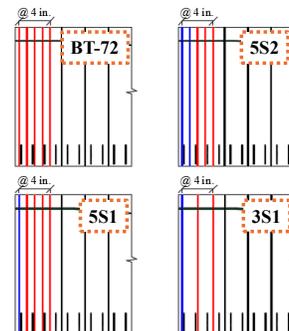
(c) End region stirrup detail

Fig. 3 Drawings and details of the BT-72 model

4.2 Numerical study of the AASHTO Type IV precast prestressed girder under live load

In the second study, which used FE modeling to assess the effectiveness of SMA transverse reinforcement for addressing end-region problems, the analysis was conducted from SMA activation through the loading phase. A section shape of AASHTO Type III with a girder length of 60 ft was designed as a reference model. **Fig. 4** shows the drawings and details of the AASHTO Type III girder model. The girder section height was 45 in., resulting in an end region length of 11.25 in. (a quarter of the girder height). In the reference model, end steel stirrups with a diameter of 0.5 in. (No. 4) were placed at 4 in. spacing to resist splitting cracks. After the end region, the equal diameter steel stirrups with 6 in. spacing reinforced the remainder of the precast prestressed girder. Confinement bars with a diameter of 0.5 in. (No. 4) were modeled up to 67.5 in. (1.5 times the girder height) from the end face of the girder with a spacing of 6 in. Twelve

prestressing strands were positioned at the bottom of the section, and four strands were at the top with a spacing of 2 in. All prestressing strands were designed to be stressed up to 75% of the ultimate strength (189 ksi). In the FE analysis of the AASHTO Type III model, all steel end stirrups were replaced with SMA stirrups to evaluate their effectiveness in service loading.
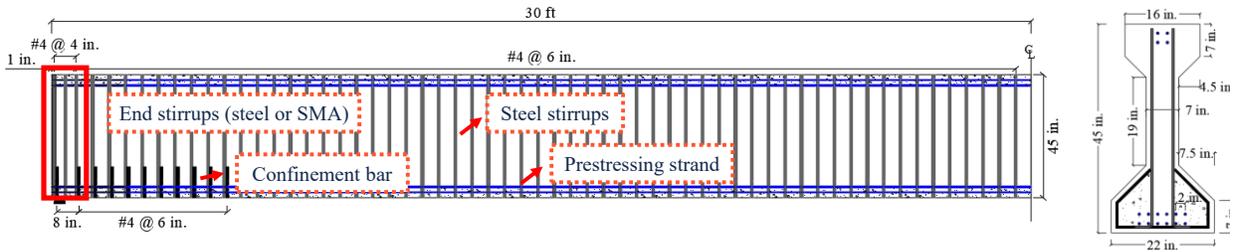

Fig. 4 Drawings and details of the AASHTO Type III model

4.3 SMA behavior during activation

Plain SMA bars with a smooth surface and a diameter of 0.24 in. were studied as the main transverse reinforcement in prestressed precast concrete girders. When employing SMA bars as stirrups, it is critical to detail them to address the lack of interfacial bonding with concrete, which may reduce the transfer of recovery stress during activation. The simplest and general method to anchor SMA bars is to hook the end tips of the bars with other reinforcements, which will resist recovery and return recovery stress. However, as shown in **Fig. 5**, when SMA is activated, the concrete resists SMA's shape recovery, inducing unwanted tensile forces in the concrete.
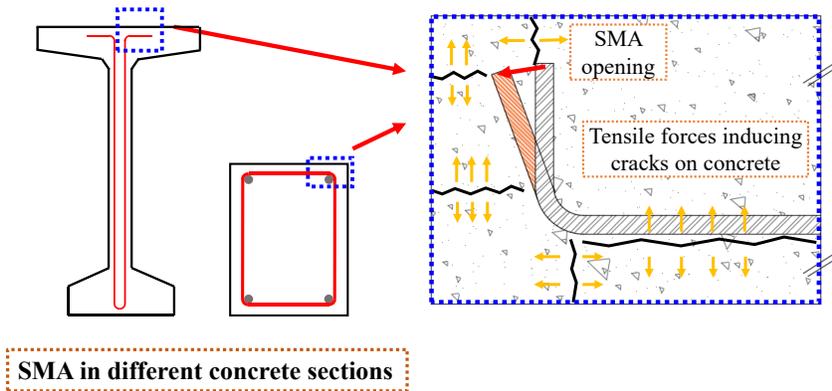

Fig. 5 SMA hook opening inside the concrete

In this part of the study, the behavior of the SMA bar during activation was experimentally investigated and numerically modeled to understand the effect of SMA opening. **Fig. 6** shows the experimental setup for evaluating SMA's opening during activation. The 90-degree SMA bar, either pre-strained or non-strained, was designed to be fixed at the straight region. The SMA bar was bent with a bending radius of 0.5 in. and extended to 1.2 in. An induction coil was used to heat the SMA bar in the bent region without affecting the straight areas. The opening displacement was measured at the indicated point (the end tip of the SMA bar) to assess opening behavior. Using experimental results, numerical modeling was also performed to better understand the strain generated at the bent region during bending and activation. The numerical modeling technique was explored to match the experimental results by following the same sequence for fabricating the bent SMA and activating (heating and cooling) the SMA bar. The numerical

analysis aimed to benefit from the investigated values in future finite element modeling to accommodate different girder end-region geometries and section shapes.
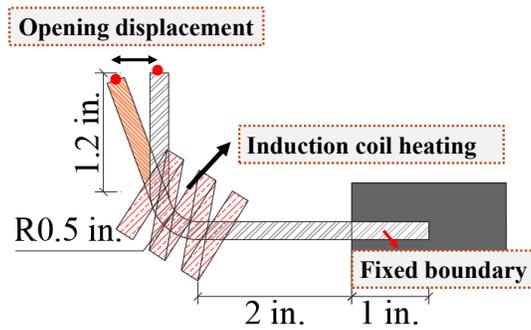

Fig. 6 SMA bar activation test setup

4.4 Activation of SMA within concrete

Following the investigation of section 4.3 of the sole SMA bar behavior, the effect of SMA bar opening behavior on the concrete was investigated in this section to secure the SMA bar's usage as an internal reinforcement. A thin concrete plate with the same thickness as the SMA bar (0.24 in.) was designed for experimental studies. The specimen dimensions are shown in **Fig. 7**. The clear cover from the SMA tip to the concrete surface was designed at 0.5 in. and 1.0 in. to assess the effect of cover thickness on preventing concrete cracking. The straight part of the SMA at the end tip was designed to be fixed with a length of 0.5 in. The region was planned as a fixed boundary throughout the activation of the SMA bar. The bent region was either pre-strained or non-strained to account for its effect on opening the SMA bar and cracking the concrete. Due to the specimen's small scale, digital image correlation (DIC) analysis was selected as the strain-monitoring tool throughout the activation of the SMA bar.
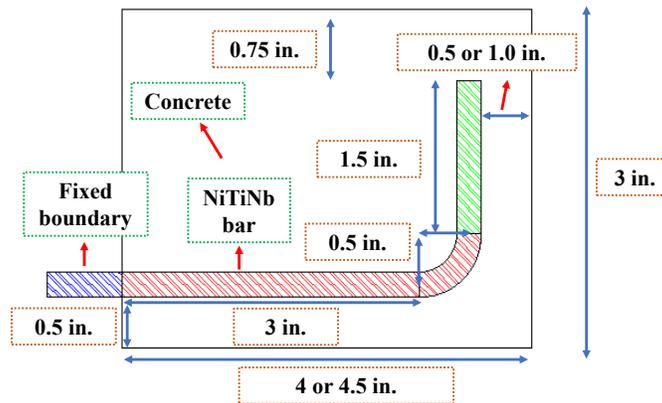

Fig. 7 Schemtaic of the SMA bar within concrete for the opening test

Numerical modeling of the SMA bar within concrete with different placements was also performed to evaluate the influence of the SMA bar opening on the prestressing force and its interaction with adjacent steel bars. **Fig. 8** shows four possible placements of the SMA bar inside the concrete, tied with steel bars. Whereas steel reinforcements are tied together, as shown in the "Typical" case, three others ("Extend", "Inner", and "Rotate") will also be investigated due to the difference in clear cover and placement of surrounding steel bars. The vertical stress at the center of the concrete was the focus of the numerical analysis, which evaluated the effectiveness of bar placement in stress recovery during SMA activation.
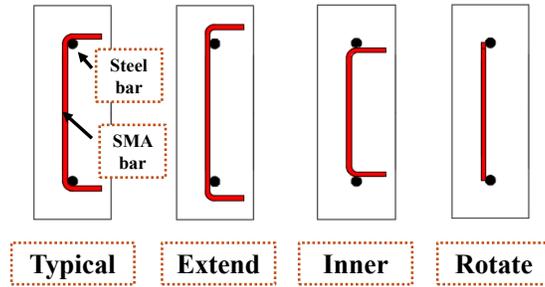
Fig. 8 SMA bar placement in reinforcement frame

4.5 Prestressing effect of SMA in small-scale specimen

The effectiveness of SMA in mitigating end region damage was experimentally studied using specimens ranging from small to large scales. In this part of the research, the prestressing effect of SMA on concrete was tested in a small-scale mortar prism. **Fig. 9** shows the drawings of the NiTiNb bar inside the mortar prism. The plain SMA bar lacked interfacial bonding with concrete; thus, it was bent 90 degrees at the end tips with an embedment length of 0.9 in. to provide anchorage of the SMA bar to concrete. The mortar prism section was 1.5 in. by 3.0 in. with a length of 14.5 in. The SMA bar was located at the mortar prism's centroid for symmetry. The SMA bar was popped out an extra 0.8 in. from the mortar to secure clamp locations for electric heating. Throughout the experiment, the distribution of recovery stress by SMA activation to the concrete was evaluated to estimate the prestressing effect.
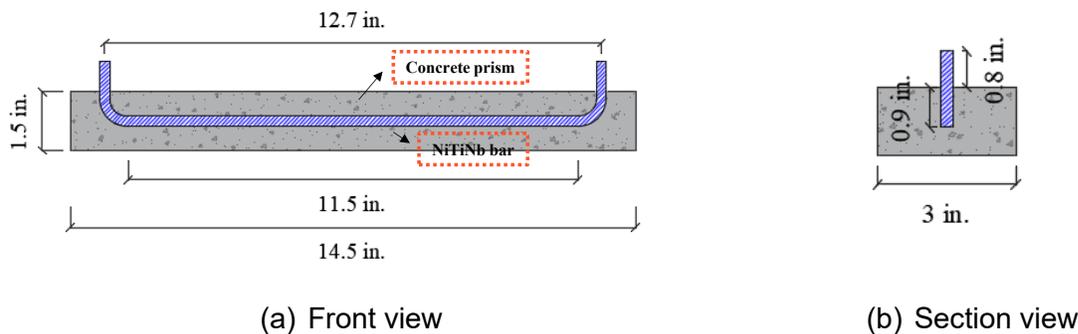

(a) Front view   (b) Section view

Fig. 9 Schematic drawings of the small-scale specimen

4.6 End region behavior of reduced-scale AASHTO Type I girder during SMA activation

The behavior of the end region during SMA activation was experimentally evaluated in a larger-scale specimen, a reduced-scale AASHTO Type I girder. **Fig. 10** shows the description of the test specimen and instrumentation plan. The prestressed precast girder was designed with a height of 14 in., a length of 36 in., a web width of 2 in., a bottom flange width of 8 in., and a top flange width of 6 in. The straight SMA was employed as vertical prestressing reinforcement in the end region ($h/4$ = 3.5 in.) of the girder, located 0.875 in. from the end face with two legs, replacing the steel stirrup. Per the AASHTO LRFD specification (AASHTO 2024), stirrups were spaced at 6 in. with a diameter of 0.25 in. (No. 2). Confinement bars should have a diameter of at least 0.375 in. according to the AASHTO LRFD specification; however, the effect of confinement bars in the experiment was negligible, which led to the manufacturing of specimens being easier by using the same dimensions and spacing of 6 in. Confinement bars were placed up to 18.875 in. to cover 1.5 times the height of the specimen (21 in.). Longitudinal bars with a diameter of 0.25 in. (No. 2)

were located at the bottom flange, with a 0.5 in. clear cover, to hold the vertical reinforcements in place during concrete pouring. All steel reinforcements were in Grade 60. To provide a more realistic boundary condition for the specimen while activating the SMA stirrup, a single seven-wire strand, with a diameter of 0.5 in. and an ultimate strength of 270 ksi, was pre-tensioned to a maximum jacking force achievable in the laboratory environment of 157 ksi. The prestressing strands provided fixity to the specimen during SMA activation. The pre-strained SMA bar, 13 in. long and 0.25 in. in diameter, was used as transverse reinforcement. The utilized SMA shows a recovery stress of 40 ksi when fully activated, and the elastic moduli in the martensite and austenite phases were 10,000 ksi and 7,500 ksi, respectively. SMA bars were crimped with bronze sleeves to improve the bond between the SMA stirrups and the surrounding concrete along their length, at a spacing of 1.5 in., until they were sufficiently secured. The SMA ends are popped out 0.5 in. from the concrete surface to connect to the electrical power supply. A K-type thermocouple is attached to the SMA surface at the center of the bar, and strain gauges (V1, V2, and V3) are installed at the surface of the specimen. Each strain gauge is at 0.875 in., 1.75 in., and 2.625 in. from the end face in the vertical direction. After conducting an SMA activation experiment, FE analysis is used to evaluate the modeling technique for SMA activation within concrete.
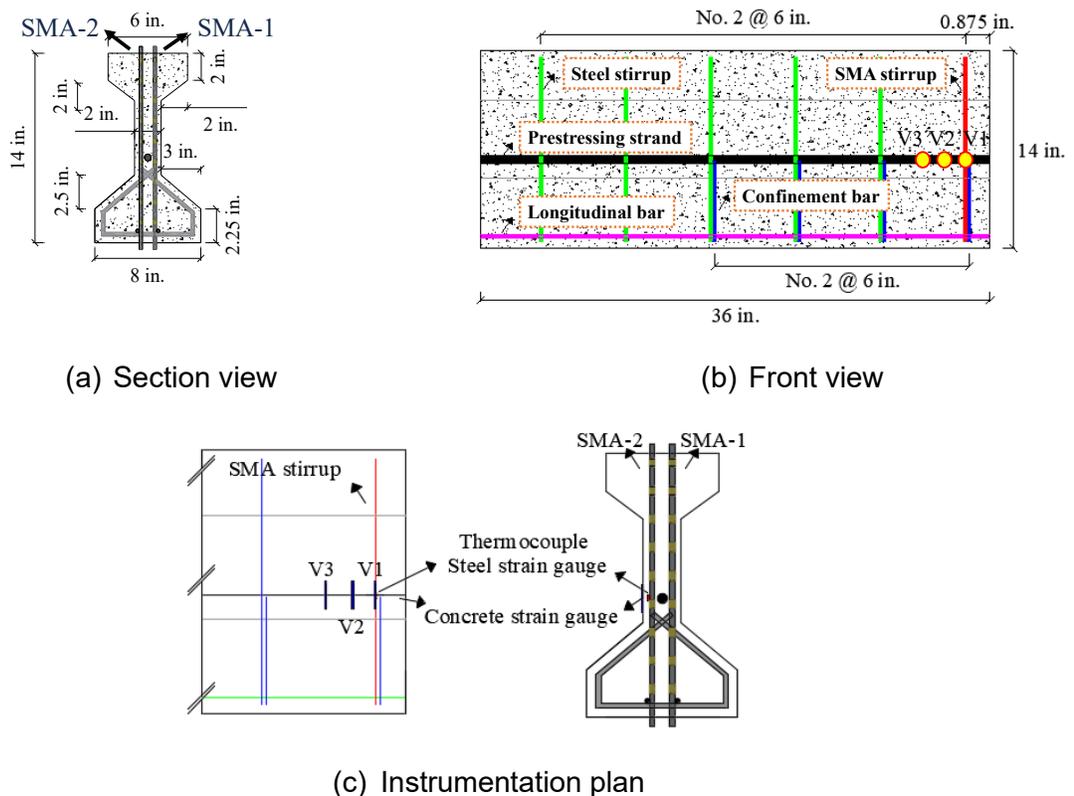

(a) Section view   (b) Front view

(c) Instrumentation plan

Fig. 10 Description of the test specimen and instrumentation plan

4.7 Crack mitigation by transverse SMA reinforcement in I-shaped precast girder
In previous tasks, from small-scale to large-scale experiments, the prestressing effect of SMA activation on the concrete surface was successfully tested using either SMA bending or adding sleeves to the surface of the SMA bar. In this part of the research, a distinct test setup was designed to assess the effectiveness of transverse SMA prestressing reinforcement in mitigating splitting cracks during prestress release. Due to limited lab conditions, reduced-scale bridge girders were manufactured without introducing prestressing strands into the specimens. Based

on previous studies (Caro et al. 2013; Ibell and Burgoyne 1993; Liao et al. 2015; Trabucchi et al. 2021), a test setup that applies a concentric load to the flange to replace prestressing forces was devised, as shown in **Fig. 11**. The girder with a certain length and height (a quarter of the length, based on AASHTO LRFD) was designed by rotating it 90 degrees. The test setup enabled the girder to experience excessive loading at the end region without necessitating a lengthy specimen to achieve sufficient prestress transfer length. A steel plate was located beneath the top flange of the girder to introduce tensile stress concentration at the web zone, which typically cracks when prestress transfer occurs on deep-height girders (i.e., BT-72). The steel plate and the fixed conditions introduced by anchor chucks were estimated to induce cantilever behavior while loading the specimen.
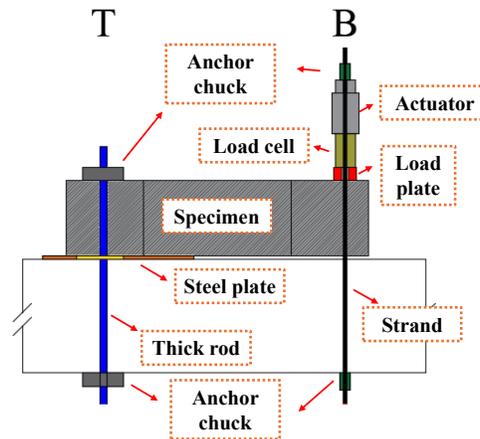

**Fig. 11** End region splitting crack test setup

Fig. 12 shows drawings of the specimens to be tested using the setup shown in **Fig. 11**. A girder specimen with a 45 in. height and 11.25 in. length, with a symmetric section, was designed for the experiments. The flange-to-web width ratio was set to 4. At the top flange, a 2-in. hole was designed to penetrate a thick rod used to fix the specimen. At the bottom flange, a 0.5-in. hole was modeled for the prestressing strand to pass through. Anchor chucks fastened the prestressing strand while locating the load plate, load cell, and actuator between them. The secured locking system, using anchor chucks, deflected the bottom flange with a manual vertical actuator, inducing tensile stress at the mid-height web. To satisfy the bursting resistance requirement specified in AASHTO LRFD (AASHTO 2024), four steel stirrups were designed at the girder specimen with a spacing of 3 in. Strain gauge instrumentation was concentrated in the web area, especially near the first and second stirrups, where cracks are anticipated to propagate. The center strain gauges (S3 and S4) were located directly above the end of the steel plate beneath the specimen, where critical damage was expected. Two additional specimens (**Fig. 12(c)**) were designed to evaluate the effectiveness of SMA transverse reinforcements in preventing splitting cracks. All SMA specimens replaced two end steel stirrups with SMA bars; however, the first specimen (SMA-1) bent the end tips and crimped sleeves on the surface of the SMA bar with a spacing of 1.5 in. The second SMA specimen (SMA-2) was designed with SMA stirrups bent only at the end tips for anchorage, without sleeves. This was to compare the efficacy of recovery stress transfer across different SMA detailing methods. The SMA specimen design was intended to assess whether steel congestion in the end region is possible with SMA transverse reinforcement.
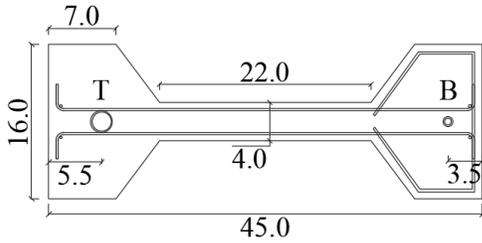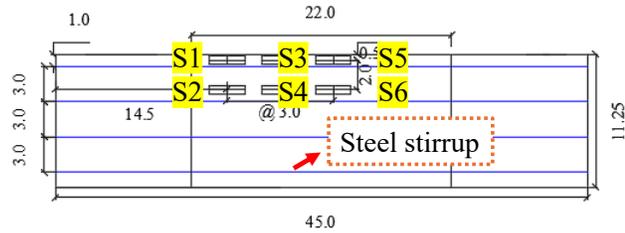
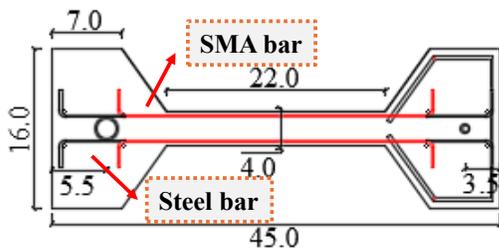(a) Section view of the rotated specimen   (b) Steel specimen
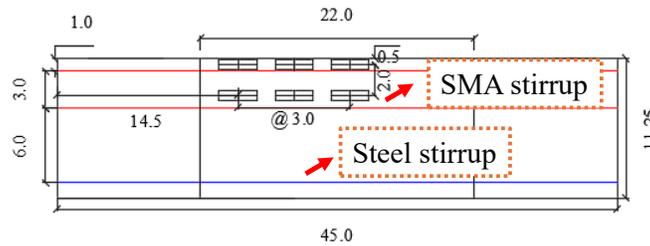
(c) SMA specimen

Fig. 12 Details of the specimens

4.8 Healing of damaged precast girder

The capability of SMA to heal the damaged precast girder was experimentally studied using the specimen design shown in **Fig. 13**. A single SMA stirrup at the far end was replaced with steel stirrups to apply prestressing force after concrete cracking. Steel stirrups were placed at the second and fourth layers of the end stirrups, with the third layer eliminated. SMA bars cover the entire web and are bent at the end tips before reaching the plastic duct, where a fixing force will be applied to the specimen. For the healing experiment, the testing sequence was modified to load the specimen and heat the SMA bar to evaluate the healing effect. The crack width and length were evaluated before and after SMA healing to assess the effectiveness of SMA in healing end region damage. An induction heating was selected as a method for heating the SMA bar. Using induction heating enabled heating the SMA bar near the cracked region first, thereby concentrating the prestressing force at the damaged area.

(a) Section view of the rotated specimen   (b) Steel specimen

Fig. 13 Healing experiment specimen design

5. Project results:

5.1 Finite element (FE) analysis on BT-72 precast prestressed girder

After the design of numerical models was finalized, FE modeling was conducted using the FE program ABAQUS software (Abaqus 2025). **Fig. 14** shows the completed numerical models of the BT-72 girder. Benefiting from the symmetry of the model, half of the length was modeled numerically to analyze end-region damage. A steel plate with pinned boundary conditions was modeled at the bottom edge of the girder as a support. Then, the steel plate was connected to the concrete using a tie-constrained connection. At the opposite end of the model, horizontal displacement and torsion were constrained. The reinforcements and prestressed strands were bonded to the concrete using the embedded-constraint method. Prestressing strands were modeled as a single wire rather than seven wires with an equivalent section area. The reinforcement element type (i.e., steel, strand, and SMA) was defined as a two-node linear 3-D truss (T3D2), and concrete was defined as an 8-node linear brick (C3D8). After mesh sensitivity tests, the mesh size was determined to be 2 in. at the end region and 4 in. at the rest region for the BT-72 girder.
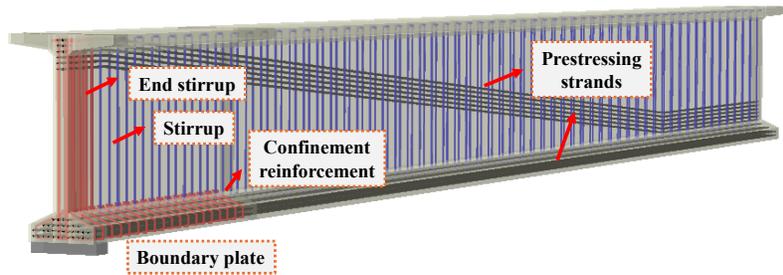

**Fig. 14** Completed BT-72 girder numerical model

The mechanical properties of concrete and steel, from the elastic to the plastic region, were defined in numerical models. **Fig. 15** shows the stress-strain relationship of each material. The compressive strength of concrete was defined as 5.8 ksi, and tensile strength as 0.49 ksi, following the equation in ACI 318-19 (ACI 318 2019). The compressive stress-strain relationship of concrete followed Hognestad's parabola (Hognestad 1951), and the tensile stress-strain curve was simplified with a trilinear curve. The concrete damaged plasticity (CDP) model was defined for the concrete plasticity property (**Table 1**), where f_{b0} is the ratio of biaxial compressive strength, f_{c0} is the uniaxial compressive strength, and K is the ratio of the second stress invariant on the tensile meridian to the compressive meridian. Steel reinforcements were modeled with 60 ksi yield strength and 90 ksi ultimate strength. For the prestressing strands, a low-relaxation strand was defined with an ultimate strength of 270 ksi and a yield strength of 243 ksi. The stress-strain curve of the SMA bar was modeled to capture recovery stress (40 ksi) with a negligible initial strain. The stress-strain relationship after SMA bar activation follows the behavior of the Austenite phase.
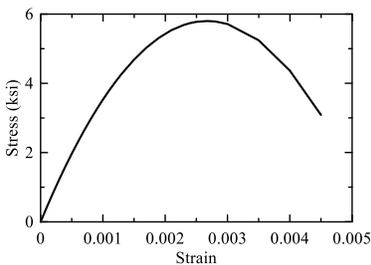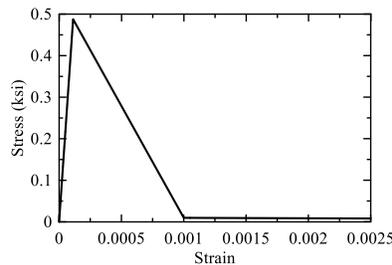
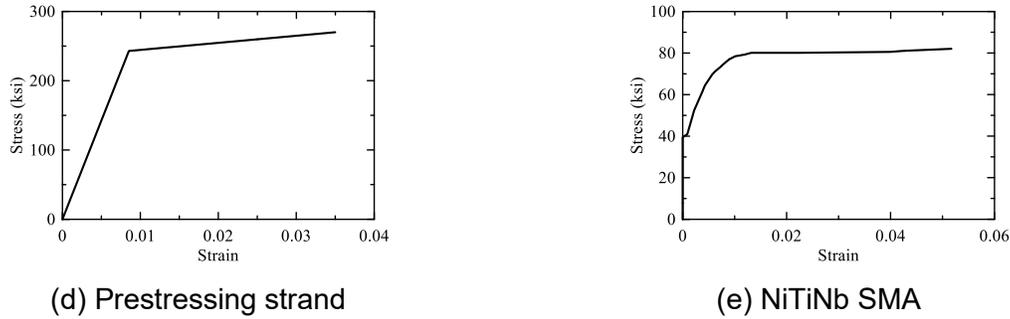(a) Concrete compressive   (b) Concrete tensile   (c) Steel

(d) Prestressing strand

(e) NiTiNb SMA
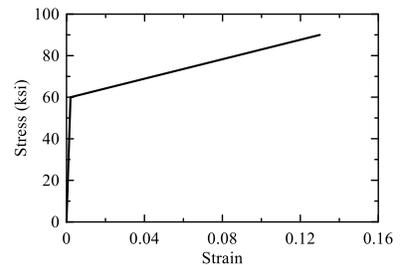
Fig. 15 Stress-strain curves of each material

Table 1. Concrete damaged plasticity (CDP) parameters

Dilation angle	Eccentricity	f_{b0}/f_{c0}	K	Viscosity parameter
31	0.1	1.16	0.67	0.001

The FE analysis was first evaluated by assessing the damage in the BT-72 precast prestressed girder. **Fig. 16(a)** shows the graphical contour of the crack pattern, where the colors are classified according to the magnitude of the tensile damage index. Red areas indicate an entirely cracked region that exceeded twice the cracking strain (230 $\mu\varepsilon$). Green regions are areas where cracks initiate (cracking strain of 115 $\mu\varepsilon$), and the blue regions are non-damaged. In the visual inspection, three major crack types at the end region were anticipated: (1) horizontal cracks at the web, (2) Y-cracks at the bottom flange, and (3) inclined cracks at the web-flange region. Based on the damage progression shown in the BT-72 model, the current steel reinforcement was insufficient to prevent crack propagation. In addition to the visual inspection, the stress distribution in the end region's steel stirrups was checked to meet the code requirement (AASHTO 2024), limiting stress to 20 ksi or less in the end region stirrups. **Fig. 16(b)** shows the stress distribution at the five end steel stirrups. Stresses were recorded at the web-flange intersections (bottom and top) and the center of the stirrup. After the prestressing strands were released, substantial stress developed as the stirrups approached the end face. In the outermost stirrup, stresses were measured at 24.1 ksi, 23.8 ksi, and 11.4 ksi from the bottom to the top. The next stirrup was subjected to stress levels of 10.3 ksi, 20.2 ksi, and 9.7 ksi. After the second stirrup, stresses reduced to below 10 ksi, satisfying the code requirement. Although the maximal stress occurred at the intersection of web and flange at the first stirrup, larger stress remained at the center of the stirrup (see second stirrup). This stress distribution resembles the crack pattern depicted in **Fig. 16(a)**.
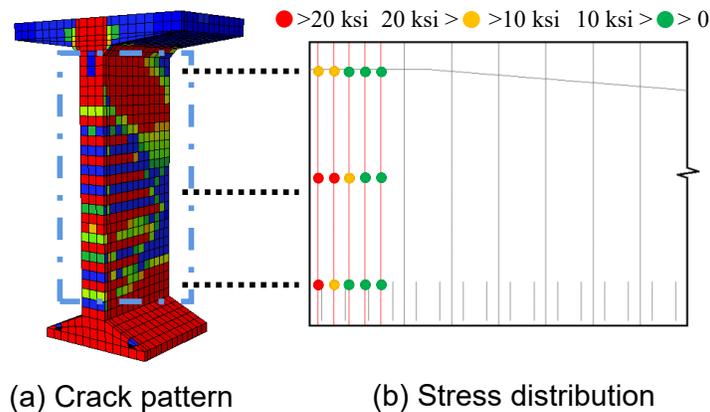

(a) Crack pattern   (b) Stress distribution

Fig. 16 Analysis results of the BT-72 model by prestress release

The effectiveness of transverse SMA reinforcement for mitigating splitting cracks was evaluated by comparing the cracked area, crack width, maximum principal strain at the web, and stress variation in end stirrups. **Figs. 17(a)-(d)** illustrates the splitting cracks in the web area of each model graphically, while **Fig. 17(e)** shows the ratio of cracked web area for different reinforcement types. The cracked area was determined based on the number of elements exceeding the maximum principal strain of 230 $\mu\varepsilon$. By contrasting BT-72 to SMA models, the horizontal web cracks in the SMA models were substantially reduced. The SMA's prestressing effect was most effective at the center and on top of the web. Additionally, less damage was found at the web-flange connections. In total, the cracked web area decreased by 25.5%, 18.6%, and 18.2% relative to the BT-72 model when comparing 5S2, 5S1, and 3S1, respectively. Inspecting the cases of 5S1 and 3S1, there was no significant difference in end region damage. As shown in **Fig. 17(b)**, the vulnerable region to prestress release is limited to a length shorter than h/4, so a single SMA stirrup may be effective enough for crack reduction.

(a) BT-72   (b) 5S2   (c) 5S1   (d) 3S1
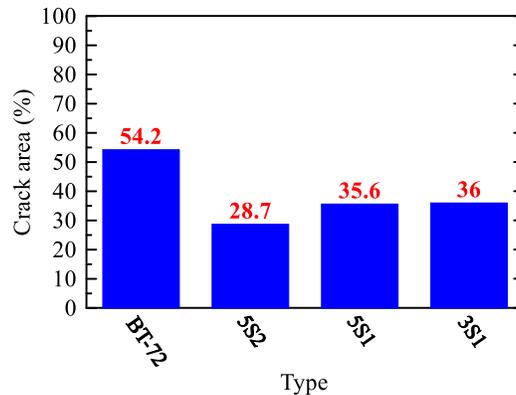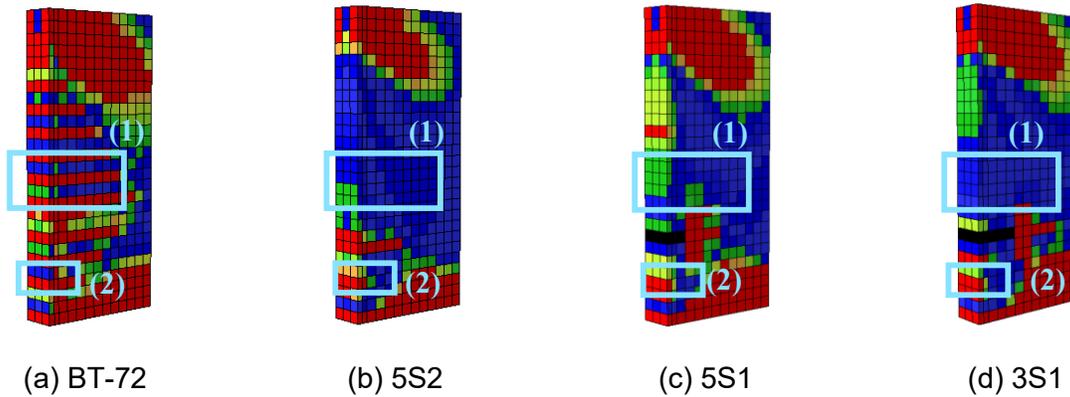
(e) Percentage of cracked elements in the web area

Fig. 17 Splitting cracks in the web of BT-72 and SMA models

Fig. 18 shows the crack width by distance for each model. The crack width at the bottom web-flange connection was measured within a distance of 4 in. from the end face (**Figs. 17(a)** to **(d)**, location (2)). According to ACI PRC 224R (ACI Committee 224 2001), BT-72 exceeded the reasonable crack widths for deicing chemicals in reinforced concrete under service loads (0.007 in.). In contrast, SMA cases fell within the acceptable range of (0.003~0.005 in.). Moreover, the cracks were nearly sealed after passing the SMA stirrup (at a distance of 2 in.). The analysis of cracking pattern and damage indicates that SMA stirrups sufficiently prevent extensive cracking in the end region of a precast prestressed girder, eventually improving serviceability (durability).
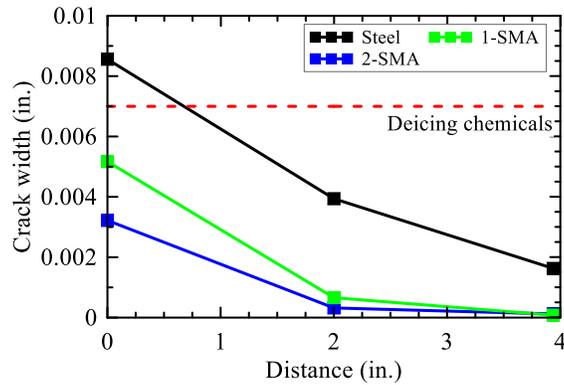
Fig. 18 Splitting cracks in the web of BT-72 and SMA models

The stress variation in end stirrups following prestress release was also evaluated to determine whether models with SMA stirrups meet AASHTO LRFD requirements (AASHTO 2024). **Fig. 19** shows the variation in stress in the end stirrups. Since SMA stirrups were stressed up to 40 ksi by activation, the stress variation was measured after the SMA activation stage. The BT-72 model showed that the two exterior layers of stirrups exceed 20 ksi. In contrast, in all SMA models, the stress variation reached less than 20 ksi. To understand the stress distribution, 10 ksi was set as the upper limit for visualizing the stress in the indicated points. As shown in **Figs. 19(b)** to **(d)**, SMA stirrups experienced negligible additional stress. Stresses developed most at the bottom of web-flange intersections, where, due to changes in section area, the SMA prestressing force was assumed to be less influential. The application of SMA led to reduced demand for stirrups.
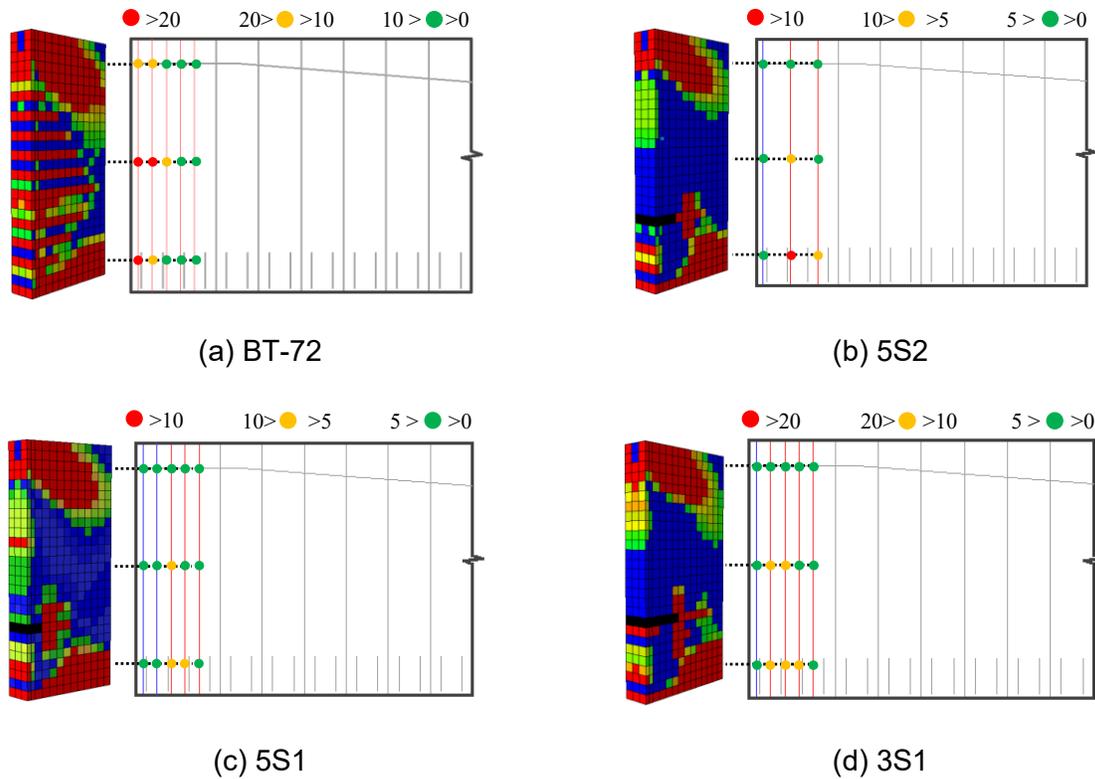

(a) BT-72

(b) 5S2

(c) 5S1

(d) 3S1

Fig. 19 Variation of stress in end stirrups

5.2 Numerical study of the AASHTO Type IV precast prestressed girder under live load

Fig. 20 shows the complete numerical model of the AASHTO Type III girder in mesh and model views. The mesh sensitivity test showed that 2 in. spacing in the end region and 4 in. spacing in the rest of the area are sufficient for analyzing the model. Two models (FEA-steel and FEA-SMA) were modeled and compared in the de-tensioning and loading phases to assess the effectiveness of SMA stirrups. The shape of the SMA stirrup was assumed to be the same as that of a steel stirrup and fully embedded in the concrete. For loading, the shear capacity of the girder was compared by positioning the load plate at the shear span-to-effective depth ratios (a/d) of 0.5, 1.0, and 2.0. Using the displacement-control method, the load-displacement curve and the tensile damage index were used as parameters for comparing performance.
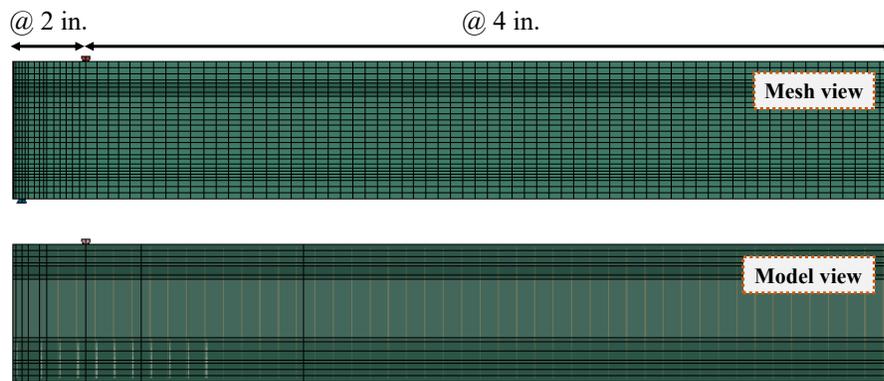
@ 2 in.   @ 4 in.

Mesh view

Model view

**Fig. 20** Schematic view of the numerical model

In the de-tensioning phase, the splitting damage at the girder web was compared between FEA-steel and FEA-SMA by monitoring the tensile damage index and vertical strain at cracking positions identified by FE analysis. **Fig. 21** shows the tensile damage index on the web of each girder model. The tensile damage index changes from blue at a cracking strain of 131.6 µε to green, then to red at a strain of 798.5 $\mu\varepsilon$. These values were decided based on the tensile behavior of concrete. The tensile damage index was visually inspected using the model's meshed view. The most vulnerable region was the shape-changing region (Location 1), which showed splitting cracks. In the FEA-steel case, the splitting crack propagated up to 11 in. from the end face, which is longer than the last end region stirrup (9 in.). In FEA-SMA, the crack extended to 5 in., where the second SMA stirrup was located. Although the SMA stirrup did not fully resist cracking at Location 1, the crack length reduced by 55%. In FEA-steel, the end splitting crack was also detected at Location 2 with a crack length of 3 in. The SMA stirrup was more effective, as shown by the absence of cracking in FEA-SMA. The vertical strain at Locations 1 and 2 was compared after releasing the prestress of 189 ksi by the distance from the end face. In Location 1, the vertical strain at FEA-steel dropped from 3,043 $\mu\varepsilon$ to 2,030 $\mu\varepsilon$ (33% drop) by passing the first stirrup at 1 in. After the second stirrup at 5 in., the vertical strain reduced from 1,770 $\mu\varepsilon$ to 1,531 $\mu\varepsilon$ (13.5% drop). For the model with SMA stirrups, the vertical strain decreased by 17.4% (from 2,238 µε to 1,849 µε) and by 52.9% (from 893 $\mu\varepsilon$ to 420 $\mu\varepsilon$) at the first and second stirrups, respectively. At Location 2, as shown in the visual inspection, FEA-SMA experienced negligible vertical strain (maximum of 168 $\mu\varepsilon$). At the first stirrup location, the vertical strain of FEA-SMA was 92.8% of the FEA-steel case, proving the effectiveness of the SMA stirrup at the end region.
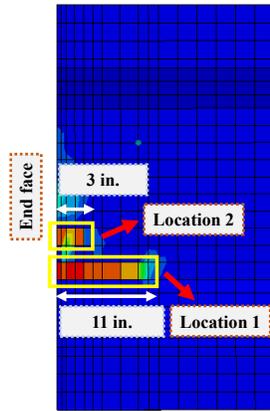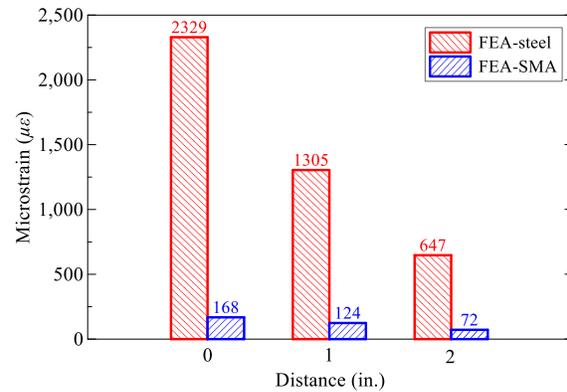
(a) FEA-steel
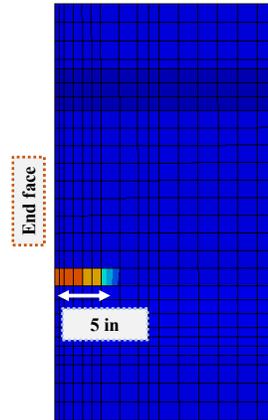
(b) FEA-SMA
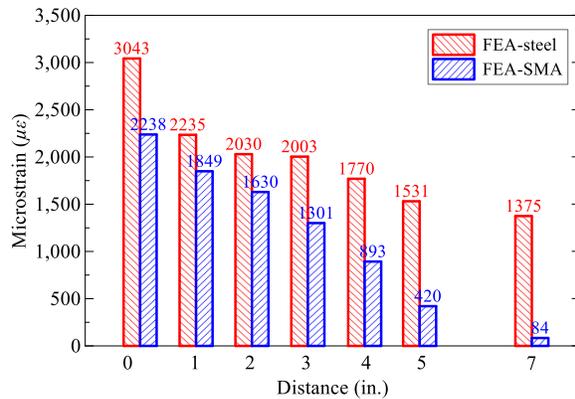
(c) Location 1 vertical strain

(d) Location 2 vertical strain

**Fig. 21** FE analysis results after de-tensioning

Fig. 22 shows the FE analysis results for the girder model loaded at shear span-to-depth ratios (a/d) of 0.5, 1.0, and 2.0. The maximum shear loads of steel and SMA models were compared to determine the effectiveness of SMA transverse reinforcement during the load stage. Damage progression of the cracking was visually detected using the damage T index based on the concrete damaged plasticity model to understand the dominant failure mode at each *a/d* ratios. In a/d value of 0.5, the maximum shear load capacity of FEA-steel and FEA-SMA was 500.6 kips and 500.5 kips, respectively, at a displacement of 0.13 in. The tensile damage index showed that diagonal shear failure is the dominant mode (**Fig. 22(a)**). In both maximum shear load capacity and crack pattern, there were negligible differences. As the a/d increased to 1.0, the shear load capacity reduced to 380.9 kips and 401.3 kips, respectively, for FEA-steel and FEA-SMA. FEA-SMA showed 5.3% better performance than FEA-steel. As shown in the tensile damage index (**Fig. 22(b)**), diagonal shear cracking remained dominant; however, flexural cracking was also observed. In a/d of 2.0, deep beam action was observed in the tensile damage index, with shear-compression failure as the dominant failure mode. More flexural cracking was detected, indicating that the beam is in a transition zone from shear failure to flexural failure behavior. The maximum shear capacity was 257.6 kips and 242.6 kips in FEA-steel and FEA-SMA at 0.77 in. and 0.70 in. displacements. In the overall FE analysis, shear capacity was similar for the steel-stirrup and SMA-stirrup models. Throughout the analysis, the feasibility of SMA reinforcement in the end regions was demonstrated to mitigate damage and improve the structure's serviceability.
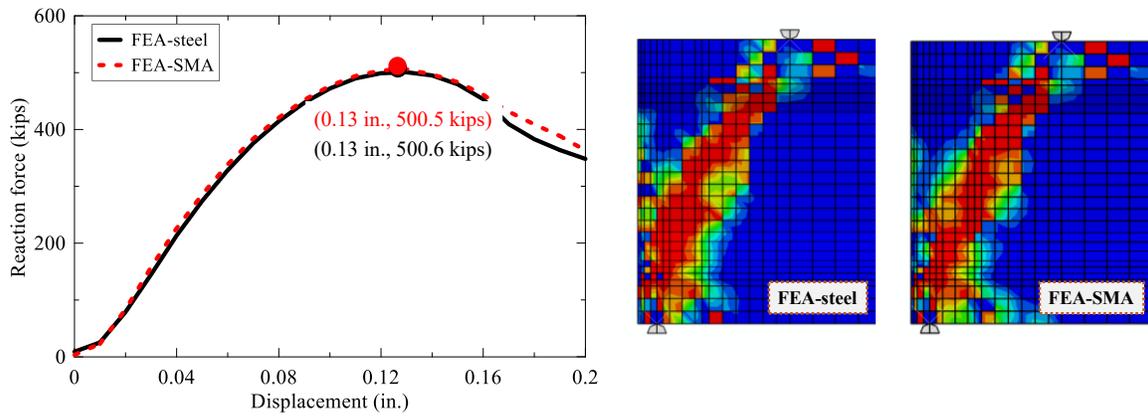
(a) a/d = 0.5
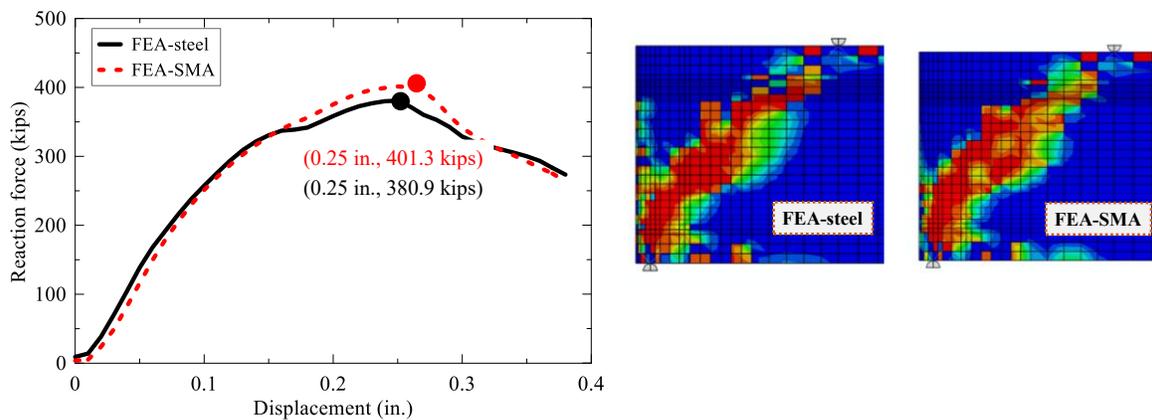
(b) a/d = 1.0
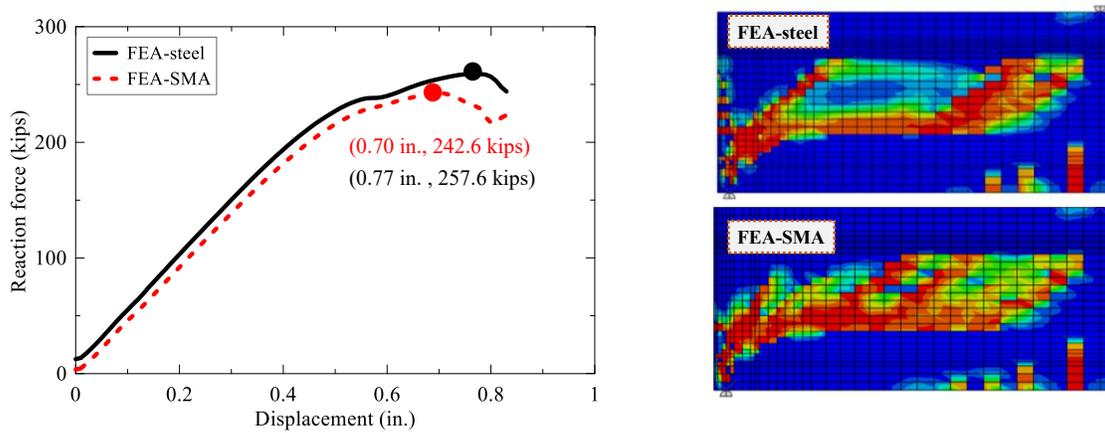
(c) a/d = 2.0

Fig. 22 Load-displacement curve by different shear span-to-effective depth ratios (a/d) and tensile damage

5.3 SMA behavior during activation

To understand the SMA behavior during activation, the experimental setup was completed as shown in **Fig. 23**. The opening range of the NiTiNb bar was investigated by bending the SMA and measuring its opening displacement by heating the bent region. Each specimen (bent only and pre-strained and bent) was fixed at the straight end. The thermocouple was attached to the center of the bent region to monitor temperature change during heating and cooling of the SMA bar. To heat the SMA bar, an induction coil with a diameter of 2.0 in. and a thickness of 0.5 in. was placed around the bent region of the bar. A small coil loop was used to avoid heating the straight area and prevent shortening due to shape recovery in that region. After heating beyond 200°C and cooling to room temperature, the opening displacement was measured at 0.25 in. and 0.7 in., respectively, for specimens 1 and 2.
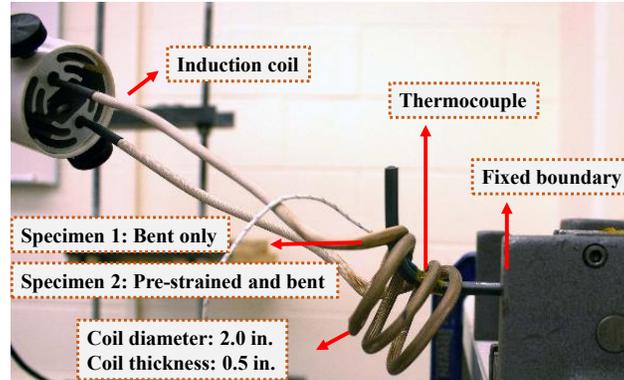

Fig. 23 Specimen of NiTiNb bar opening test

Fig. 24 shows the procedure of SMA opening during activation. When SMA bars are bent, compressive strain develops at the inner section, whereas the outer section experiences tensile strain. During activation, shape recovery restores the bar's original shape, generating tensile strain in the inner section and compressive strain in the outer section. If the SMA bar is pre-strained, more compressive strain is applied throughout the bar, resulting in more compression to the outer section. There is less tensile strain occurring at the inner section; however, due to the larger area at the outer section, more opening displacement appears with the pre-strained specimen. As shown by the experimental results, the opening displacement in Specimen 2 was 178% more than in Specimen 2. Thus, it was noted that avoiding pre-straining the bent region of the SMA would be recommended.

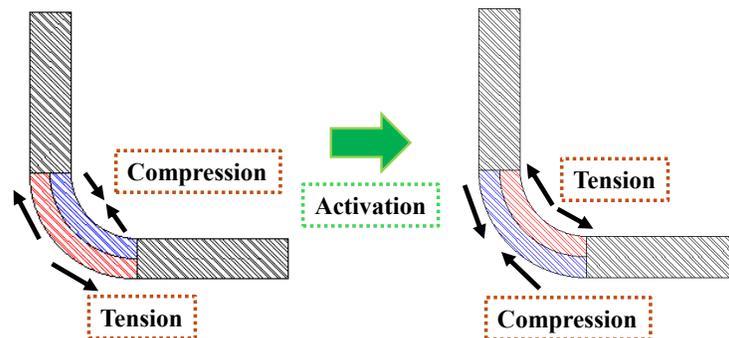**Fig. 24** SMA bar opening process

Based on experimental results, numerical modeling was performed to quantify the strain generated at the bent region of the SMA bar by activation. Since the opening of the SMA bent region involves different levels of recovery strain across the bar section, the bar's section was segmented into four parts, and four different thermal coefficients were assigned to each segment.

To achieve the target strain, numerical analysis was performed in the sequence shown in **Fig. 25**. First, the induced strain at the bent region was obtained by averaging the values across each section after applying an external force to bend the SMA bar. Then, thermal coefficients were defined based on the achieved strain values to induce SMA opening during activation. **Fig. 26** shows the finalized thermal strain of Specimen 1 and Specimen 2 numerical models. By the allocated thermal strain, each specimen exhibited an opening displacement of 0.27 in. (Specimen 1) and 0.70 in. (Specimen 2) after activating the SMA bar. The accuracy of the finite element analysis (FEA) results to experimental results was 92% and 100%, respectively, modeling the 90-degree hook opening of a NiTiNb bar with a diameter of 0.24 in. and a bending radius of 0.5 in., which is acceptable when using the suggested values.
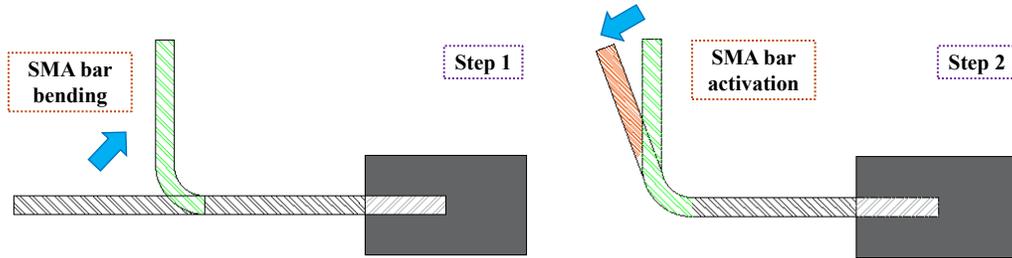
Fig. 25 Bending and activating the SMA bar

Section 1: $\varepsilon_T = 1.6 \times 10^{-4}$
Section 2: $\varepsilon_T = 6.4 \times 10^{-4}$
Section 3: $\varepsilon_T = -3.1 \times 10^{-4}$
Section 4: $\varepsilon_T = -7.7 \times 10^{-4}$

(a) Specimen 1

Section 1: $\varepsilon_T = 7.1 \times 10^{-5}$
Section 2: $\varepsilon_T = 6.9 \times 10^{-4}$
Section 3: $\varepsilon_T = -7.2 \times 10^{-4}$
Section 4: $\varepsilon_T = -1.4 \times 10^{-3}$
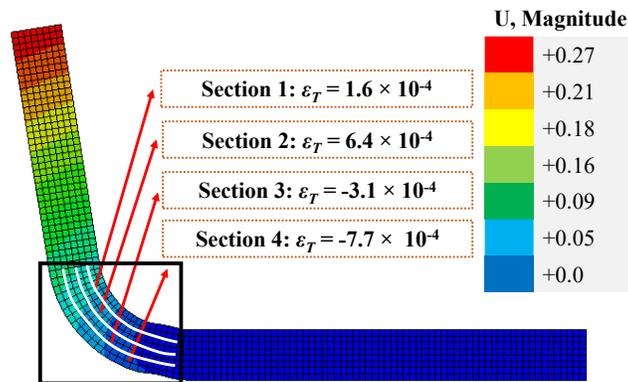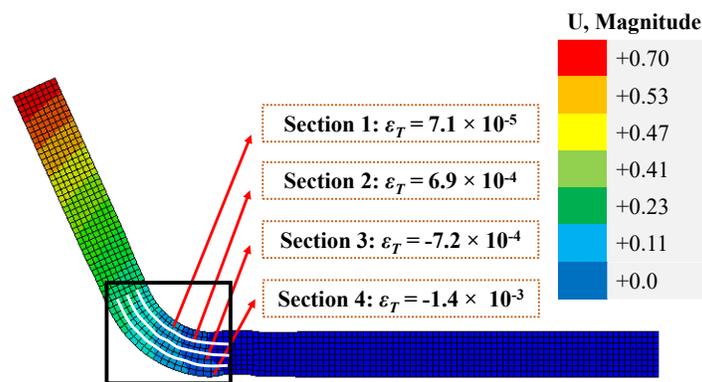
(b) Specimen 2

Fig. 26 Thermal strain assigned for sections

5.4 Activation of SMA within concrete

The opening effect of SMA on concrete was experimentally investigated using four specimens with different clear cover and pre-straining levels in the bent region. **Fig. 27** shows the manufactured molds for the thin concrete specimen and the concrete casting procedure. The specimens were labeled as "B1", "B2", "PB1", "PB2", where "B" stands for specimens with bending only, "PB" denotes pre-straining and bending, "1" for specimens with a clear cover of 0.5 in., and "2" for specimens with a clear cover of 1.0 in. **Fig. 28** shows the representative test setup for activating the SMA bar within concrete. As DIC analysis was selected to monitor strain variation, speckle patterns were acquired on the front face of the specimen. The SMA bar was heated from the heat gun at the back to avoid damaging the speckle patterns.

| (a) Specimen molds | (b) Concrete casting |

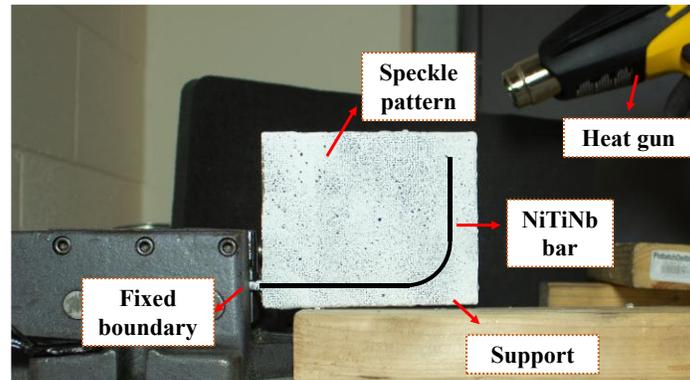**Fig. 27** SMA within concrete specimen manufacturing process

Fig. 28 SMA bar within concrete test setup

Fig. 29 shows the results of experiments in which SMA was heated beyond 200°C. In DIC results, the red, orange, and yellow regions indicate the tensile strain-subjected zones, whereas blue and purple represent the compressive strain-subjected zones. Except for the B2 specimen, which was made with a bent only SMA bar and a clear cover of 1 in., all specimens were fractured due to the SMA opening. In B1 specimen (**Fig. 29(a)**), the tensile strain was captured where the bending of the SMA was terminating and at the end tip of the SMA. A slight tensile strain was also captured at the straight region of the SMA. From the fractured view of the B1 specimen, due to the discontinuity after the SMA end tip's concrete cracking, the upper part blew out. In the B2 specimen (**Fig. 29(b)**), the tensile strain was generated in a similar region to the B1 specimen, whereas a sufficiently clear cover of 1 in. prevented the concrete from cracking. In visual

inspection of the specimen, there was no symptom of minor cracking. In PB1 and PB2 cases (**Figs. 29(c)** and **(d)**), the splitting cracks mainly propagated along the straight part of the SMA. The increased opening force from pre-straining and bending might have made the uplift force greater than the tensile strength of the concrete, resulting in splitting cracks. Since the dominant failure occurred in the straight part, increasing the clear cover was not effective in preventing cracks by SMA activation. Minor cracks were also formed at the bent region's starting or ending point. With a lower opening force, the bent region and end tip were more susceptible to cracks, implying that sufficient cover would make it possible to resist cracking, as shown in the B2 specimen.
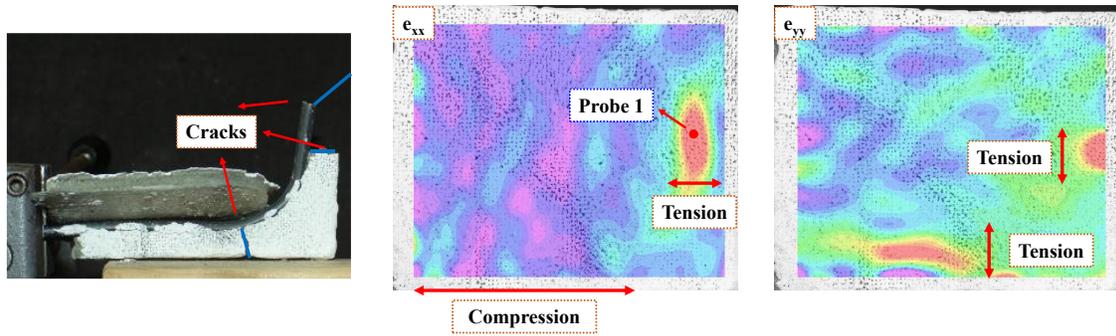
(a) B1
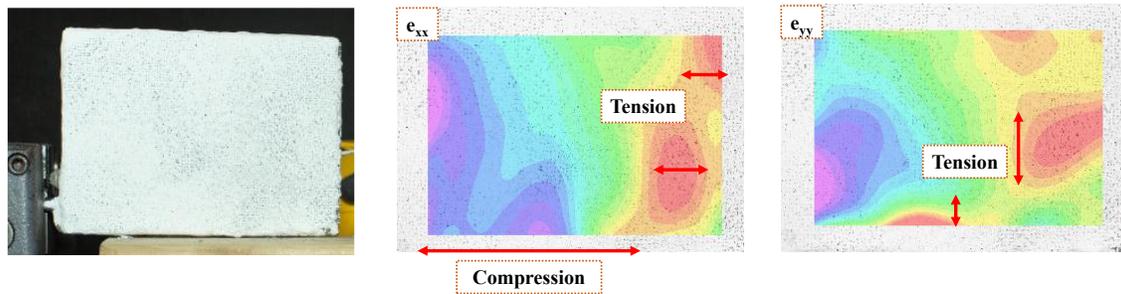
(b) B2
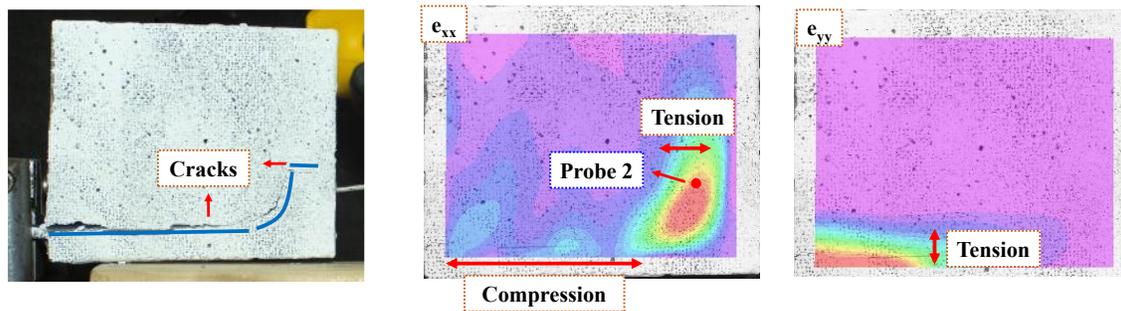
(c) PB1

(d) PB2

Fig. 29 Test results of SMA opening by activation inside specimens
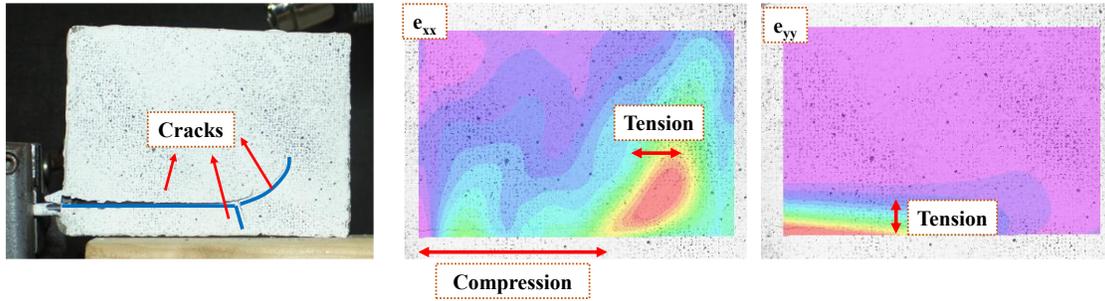
The specimens of B1 and PB1 were numerically modeled using the modeling technique mentioned in section 5.3. This method divided the bent region of the SMA into four segments and applied the thermal coefficient to each segment to capture the opening effect. Finite element analysis (FEA) results were compared with DIC analysis (experimental results) to verify the accuracy of the numerical results and assess the impact of SMA opening. The strain histories were analyzed at Probe 1 (**Fig. 30(a)**) and Probe 2 (**Fig. 30(b)**), where DIC analysis showed a tensile strain developing and eventually cracking during the heating of the SMA bar in the bent region. In the FEA, the nodal strain was measured at the indicated point. Throughout the comparison between DIC analysis and FEA results, both horizontal (e_{xx}) and vertical (e_{yy}) strain variations were nearly coincident, validating the numerical modeling method. In the strain history measured by Probe 1 (B1 specimen), heating the SMA induced tensile strain in the area. After heating to 160°C, e_{yy} shifted from compressive strain to tensile strain, indicating that the concrete started to crack. In Probe 2 (PB1 specimen) monitoring, pre-straining of the bent region resulted in an initial compressive strain in the e_{xx} history. However, after reaching 160°C, it exhibited tensile strain, and the concrete began to crack.
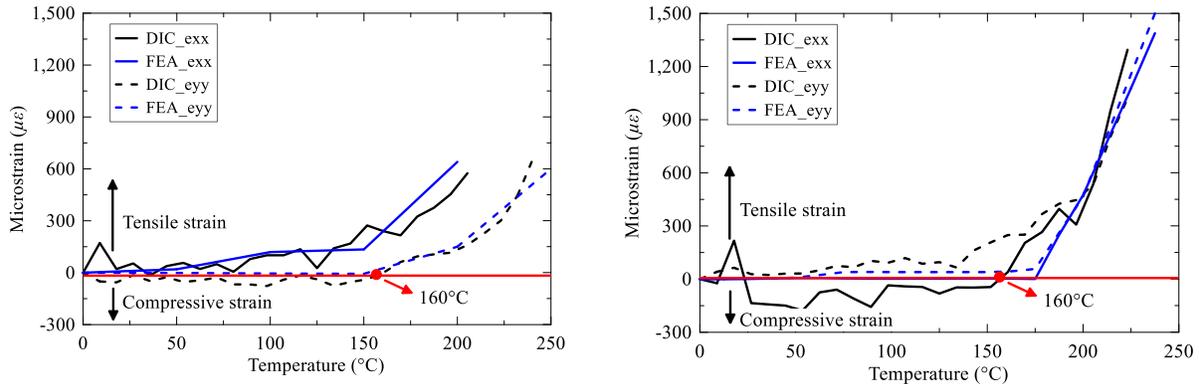
(a) Probe 1 strain history (B1 specimen)　(b) Probe 2 strain history (PB1 specimen)

Fig. 30 DIC and FEA analysis results

5.5 Prestressing effect of SMA in a small-scale specimen

Fig. 31 shows the test setup and instrumentation of the small-scale specimen. In the electric heating of SMA bar, the power supply generates the electric current and directly sends it through the SMA bar by connecting alligator clamps to the end tips of the SMA (**Fig. 31(a)**). A K-type thermocouple was installed at the center of the SMA bar within the specimen and protruded to

the mortar's top surface. The temperature reader recorded the temperature variation during the heating and cooling of the SMA. A speckle pattern was scattered at the front face for digital image correlation (DIC) analysis (McCormick and Lord 2010). The DIC analysis was capable of detecting the strain contour on the applied surface. Speckle patterns had a dot size of 0.014 in. Four strain gauges were attached to the mortar at equal spacing and connected to the data acquisition system, which measured the concrete strain variation along the longitudinal axis of the specimen. Strain data were obtained parallel to the SMA at curved and straight parts to evaluate the recovery stress (prestress) during the SMA activation. Strain gauges are labeled G1, G2, G3, and G4 (**Fig. 31(b)**).
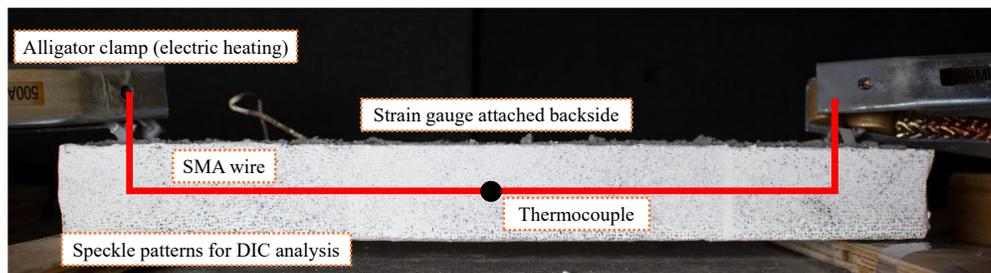
(a) Front face of the specimen

(b) Rear face of the specimen

Fig. 31 Test setup for electric heating of SMA in mortar

The prestressing effect of SMA during activation was evaluated by measuring concrete strain with strain gauges and DIC analysis, while monitoring the temperature variation of the NiTiNb bar. **Fig. 32** shows the test results measured by strain gauges and DIC. G1 and G3 each represent the concrete strain variation at the concrete surface parallel to SMA's bent and straight regions. The concrete compressive strength measured by the concrete cylinder test was 6.2 ksi with an elastic modulus of 3,380 ksi. After the heating of the SMA started, compressive stress was first generated at the concrete surface near the SMA bent region. In strain gauge G1, the maximum compressive strain of -120 $\mu\varepsilon$ was measured at SMA temperature of 190°C. After reaching the maximum compressive strain, SMA opening under tensile force at the bent region reduced the compressive strain to -13 $\mu\varepsilon$ after cooling to room temperature. The strain development trend observed in the G1 strain gauges was similar to that shown in the DIC analysis (DIC-B curve). In the DIC-B curve, the maximum strain measured in the concrete reached -140 με, then decreased to -30 με. Throughout the experiment, it was shown that the SMA activation first generated compressive strain at the bent region. Still, due to SMA recovery to its original straight shape, tensile forces were induced in the concrete after full SMA activation. At the center of the mortar prism, thermal expansion of the SMA initially induced tensile strains. The maximum tensile strain measured by the strain gauge (G3) and DIC analysis (DIC-C) was 26 $\mu\varepsilon$ and 9 $\mu\varepsilon$, respectively. As the SMA heating reached its maximum temperature of 200°C and cooled down, thermal compression and the shape memory effect induced compressive strain at the surface of the concrete, reaching -120 με and -130 με, respectively, according to the strain gauge (G3) and

DIC analysis (DIC-C). The utilized pre-strained NiTiNb SMA was expected to exhibit a recovery stress of 40 ksi by full activation. This full recovery stress of the SMA was expected to produce a compressive strain of -130 µε at the center of the mortar, which was nearly identical to the experimental results. Thus, the bent plain SMA with smooth surface was sufficient to transfer full recovery stress to the small-scale mortar prism even if located inside the mortar without thermal insulation.
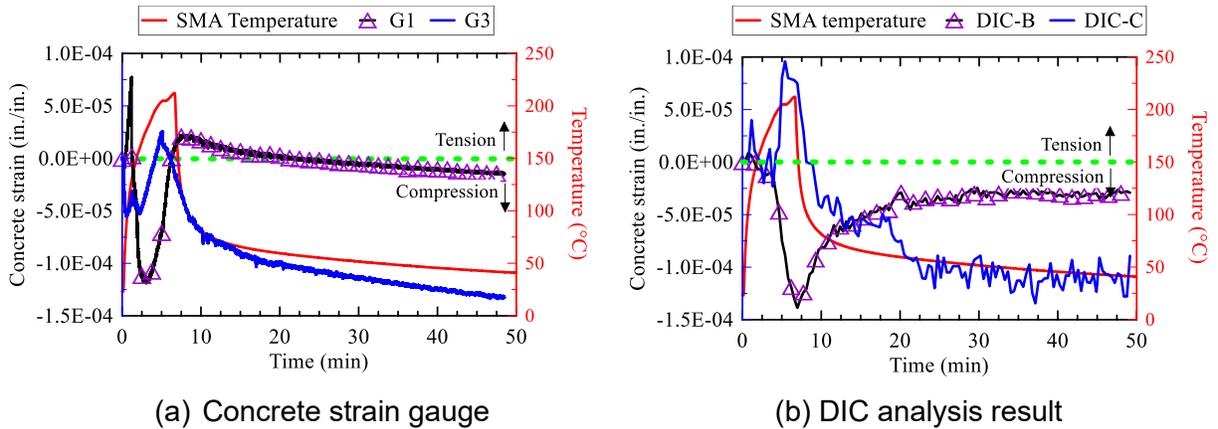

(a) Concrete strain gauge   (b) DIC analysis result

Fig. 32 Test results of SMA activation in a small-scale experiment

Fig. 33 illustrates the strain flow at the mortar surface determined using the DIC analysis. The strain applied to the mortar surface varied from -150 µε to 10 µε along the SMA bar. Although the specimen was designed to be symmetric, as discussed in the data of the G1 strain gauge and DIC-B, SMA activation induced opening at the specimen's right side, resulting in tensile strain on the mortar. The tensile strain disturbed the distribution of compressive strain built by SMA activation, but increased from the left end to the right end. However, except at one end of the SMA bent region, the measured compressive strain was in the range of -150 µε to -100 µε.
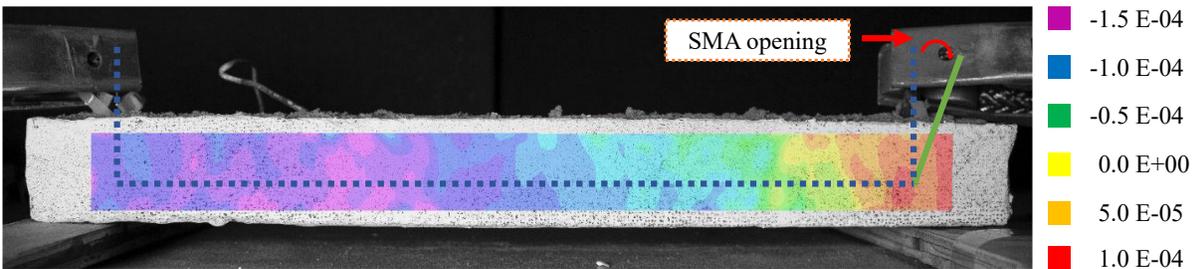

Fig. 33 Strain flow at the mortar surface detected by DIC analysis

5.6 End region behavior of reduced-scale AASHTO Type I girder during SMA activation
The effectiveness of SMA transverse reinforcement in mitigating splitting cracks was experimentally evaluated using a reduced-scale AASHTO Type I girder. To manufacture prestressed concrete, the method of stretching and releasing the strands was first explored with a single prestressing strand fixed at the test setup. **Fig. 34** shows the jacking and releasing procedure of the strands. Due to limited lab conditions for placing the prestressing bed, a short prestressing strand, 3 ft long, was fixed using anchor chucks. A monotonic actuator was used to stretch the strands. During strand stretching, the strands were stretched to 30 kips, corresponding to a prestress of 196 ksi. After jacking, the actuator was removed with an initial prestressing force loss of 7 kips, resulting in 23 kips (150 ksi) of prestressing force (stress) remaining in the

prestressing strand. A flame-cutting method for rapid prestress transfer was investigated to release the prestressing force. By adjusting the flame intensity, it was able to cut each strand within 30 seconds, which was desirable to transfer prestress without elongating the strands due to thermal expansion or to avoid excessive impact from instantaneous cutting.

(a) Jacking   (b) Releasing

Fig. 34 Pre-tensioning process of a prestressing strand

After conducting experiments on the pre-tensioning process for prestressing strands, a specimen with SMA stirrups in the end region was manufactured, as shown in **Fig. 35**. Two straight SMA bars were installed in the end region, with sleeves crimped to the surface of the SMA, spaced 1.5 in. apart. Wood spacers maintained the spacing of the two legs of each stirrup. All stirrups were tied to the bottom longitudinal bar and the stretched prestressing strand to secure their locations (**Fig. 35(b)**). To create an I-shape during the pouring of concrete, styrofoam was attached to the wooden side face. Due to the distance between the concrete lab and the prestressing location, a self-consolidated concrete (SCC) mix was used for concrete casting. It enabled the concrete to flow sufficiently inside the specimen mold without any vibration.

(a) SMA stirrup   (b) Reinforcement assembly

| (c) I-shape mold | (d) Concrete pouring | (e) Concrete casting |

Fig. 35 Manufacturing process of reduced-scale AASHTO Type I girder

The designed reduced-scale AASHTO Type I girder was fabricated as shown in **Fig. 36**. The end tips of the SMA bars protruded to connect them to the alligator clamps that conduct electricity. The prestressed strands fixed the specimen in position with concrete blocks supporting the specimen. As shown in **Fig. 36(b)**, three strain gauges were attached at the end region of the girder after smoothing the surface and applying epoxy-adhesive. The SMA activation test was conducted three days after concrete casting, noting that strand cutting typically occurs within a few days of casting. The compressive strength of the concrete at the test date was measured as 8.5 ksi, with a 28-day strength of 10.4 ksi based on the cylinder compression test.
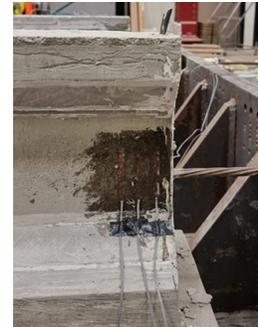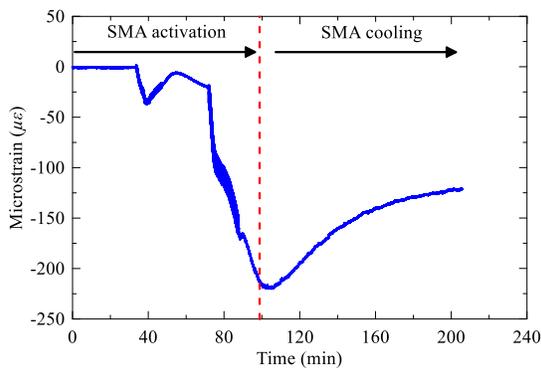

| (a) Test specimen | (b) Strain gauges |

Fig. 36 Manufactured specimen

Fig. 37 shows the test results during SMA activation. Two SMA bars (SMA-1 and SMA-2) were heated separately using the electric heating method, starting from the far side of the concrete strain gauge (1.5 in. from the concrete surface, SMA-1) to the nearest bar (0.5 in. from the surface, SMA-2). SMA bars were heated above 200°C to activate NiTiNb fully, then cooled to room temperature. As shown in **Figs. 37 (a)** to **(c)**, after heating the SMA bars, the strain recorded in V1, V2, and V3 strain gauges was -205$\mu\varepsilon$, -220$\mu\varepsilon$, and 8$\mu\varepsilon$, respectively. However, after the SMA and concrete cooled to room temperature for 2 hours, the compressive strain stabilized at -121 $\mu\varepsilon$, -75 $\mu\varepsilon$, and -35 $\mu\varepsilon$. Based on the concrete cylinder compression test (**Fig. 37(d)**), the compressive stress applied in V1, V2, and V3 after cooling corresponds to 0.91 ksi, 0.56 ksi, and 0.26 ksi. Theoretically, for the recovery stress of 40 ksi assumed for the SMA, the compressive strain (stress) induced by SMA stirrup at V1 location was estimated to be -110 $\mu\varepsilon$ (0.83 ksi). The

theoretical value was calculated by **Eq. 1**, where σ_r is the recovery stress (40 ksi), A_{SMA} is the total cross-sectional area of SMA bars (0.1 in^2), E_c is the elastic modulus of concrete (5,767 ksi), and A_c is the effective area of concrete (6 in^2). The theoretical value and experimental results differed by only 10%, indicating that, with appropriate bonding between SMA and concrete, the recovery stress of SMA upon activation can be fully transferred to the concrete as prestress. It is also noted in **Fig. 37(e)** that the prestressing force by SMA activation was maximum at the location of SMA, linearly dropping down with distance. Based on the strain level measured at three locations, a linear equation (Eq. 2) is derived, where x is the distance from the SMA stirrups (in.), and $\varepsilon_{SMA,y}$ is the vertical strain induced by SMA activation. In **Eq. 2**, it was found that a single SMA stirrup with two legs was influencing up to 2.4 in. from the SMA reinforcement

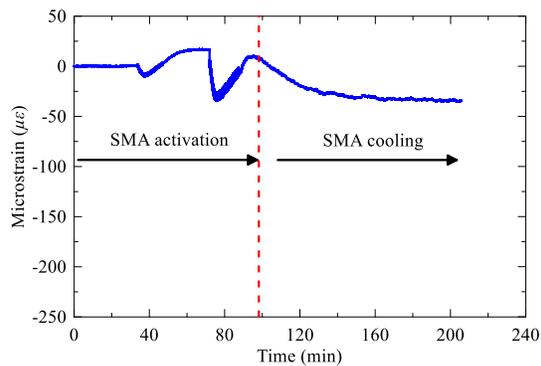$$\varepsilon_{comp} = \frac{\sigma_r \times A_{SMA}}{E_c \times A_c} \tag{1}$$

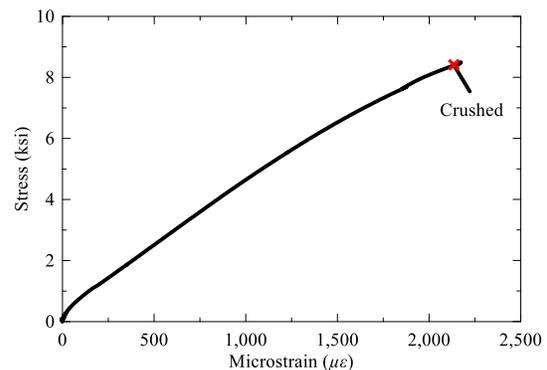$$\varepsilon_{SMA,y} = -1.93x + 120 \tag{2}$$
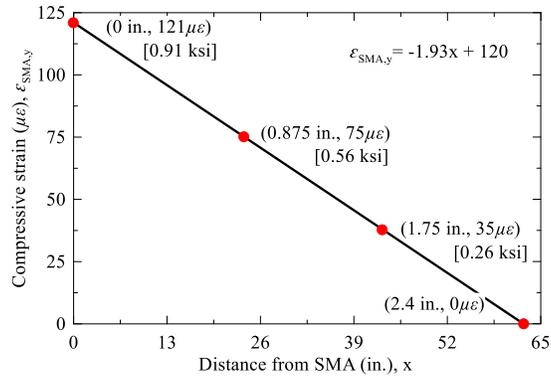

(a) V1 strain gauge
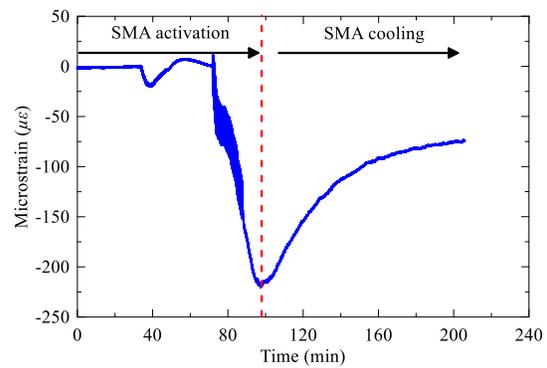

(b) V2 strain gauge

(c) V3 strain gauge

(d) Concrete compressive stress-strain curve

(e) SMA activation influence line

Fig. 37 Test results during SMA activation

Fig. 38 shows the numerical model of the test specimen. The mechanical material properties were defined identically to the test specimen. The element types for the SMA stirrup and steel stirrup were defined as a 2-node 3-D truss, an 8-node linear brick (C3D8) for concrete, and a 2-node linear beam (B31) for prestressing strand. The plasticity model of concrete was defined as a CDP model. The contact behavior between the boundary and the specimen was defined as hard contact for normal behavior and a friction coefficient of 0.7 for tangential behavior. The numerical model mesh was set to 0.4375 in. cubic after mesh sensitivity tests.
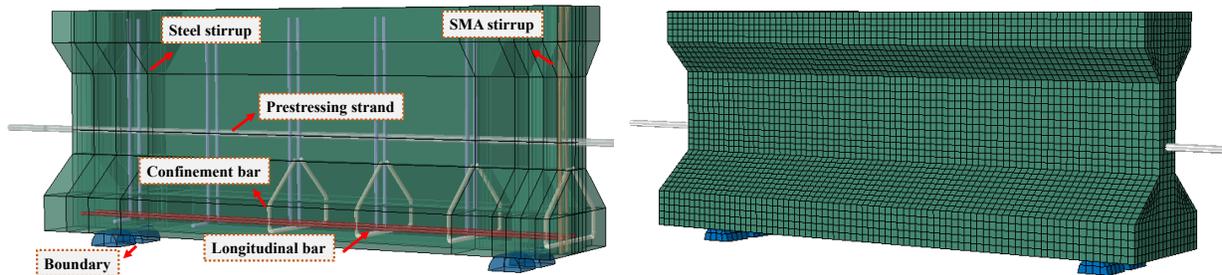
(a) SMA activation girder model   (b) Meshed model view

Fig. 38 Numerical model for SMA activation girder experiment

In the FE analysis, SMA activation was modeled using thermal expansion to induce a recovery stress (prestress). During the analysis, SMA was embedded in the concrete, with negative thermal expansion of SMA as its temperature increased. By subjecting SMA to shrinkage, the concrete resisted it through complete bonding, resulting in compressive stress along the effective area. **Fig. 39** compares the experimental and FE analysis results for the SMA activation at V1, V2, and V3 concrete strain gauge locations. In FE analysis, the measured values were 111.8 $\mu\varepsilon$, 77.5 $\mu\varepsilon$, and 35.6 $\mu\varepsilon$, with an average difference of 4.2%, indicating the accuracy of the numerical modeling method.
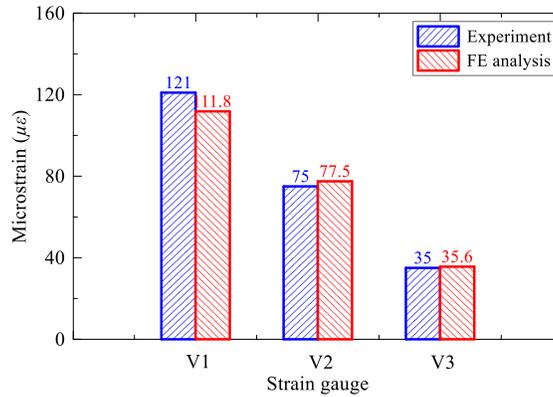
Fig. 39 SMA activation results of experiment and FEA

5.7 Crack mitigation by transverse SMA reinforcement in I-shaped precast girder

Fig. 40 shows the manufacturing process of each specimen. Plastic ducts were used to secure the hole for the penetrating steel rod and prestressing strand. Four longitudinal bars formed a steel frame to secure transverse reinforcements in place. In SMA specimens (**Figs. 40(b)** and **(c)**), k-type thermocouples were attached to the surface of the SMA bar to monitor temperature variation during the heating and cooling of the SMA bar. For specimen SMA-1 (**Fig. 40(b)**), the SMA bars were bent along the confinement bar, and an extra confinement bar was placed at the top flange to fix the SMA bars in position. Because the experimental setup was designed to concentrate stress on the web, adding a confinement bar was expected to have a negligible effect. For the SMA-2 specimen, the SMA was bent to 90 degrees without adding sleeves. This setup enabled the investigation of the recovery stress transfer ability of sole SMA bending in a large-scale specimen.
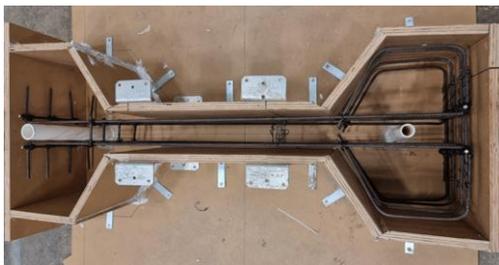
(a) Steel specimen mold
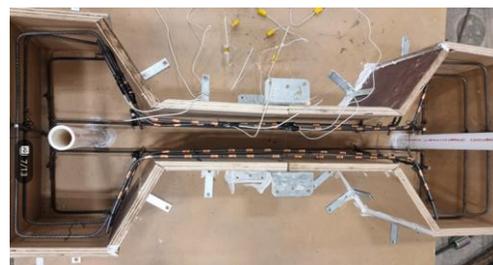
(b) SMA-1 specimen mold

(c) SMA-2 specimen mold

Fig. 40 Specimen molds and completed test setup

The SMA activation of specimens SMA-1 and SMA-2 was conducted using the induction-heating method. A self-made rectangular induction coil with two loops was fabricated to heat the SMA bar in the web area (**Fig. 41(a)**). After the heating of SMA and cooling of SMA and concrete, the compressive strains measured by strain gauges were averaged by the position (i.e., S1 and S2) to estimate the prestressing effect. **Fig. 41(b)** shows the results of SMA activation. Adding sleeves to the surface of the SMA bar generally resulted in higher transfer of recovery stress. The compressive strain built in SMA-1 was 41 $\mu\varepsilon$, 81.5 $\mu\varepsilon$, and 56 $\mu\varepsilon$ at each layer, whereas SMA-2 showed 46% lower strain (19 με), 56% lower strain (46 με), and 46% lower strain (26 με). It is estimated that, as the anchorage of SMA bars was formed at the flange area, the prestressing force by SMA activation was transferred from the wide flange. When using sleeves, each sleeve acted as an anchorage region, transferring recovery stress to the narrower web area. Thus, the measured prestressing strain dropped 50% on average.
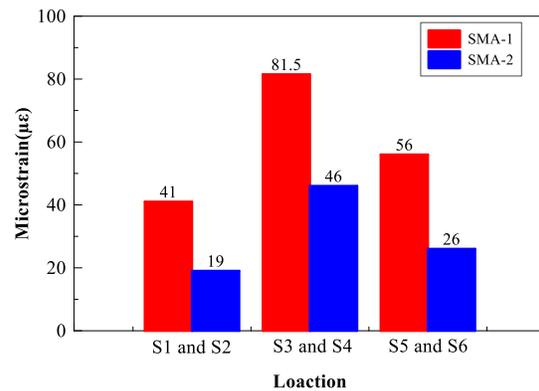
(a) SMA activation using induction heating

(b) Averaged compressive strain

Fig. 41 SMA activation test results

After activating SMA bars in SMA-1 and SMA-2 specimens, loading tests were conducted to compare the cracking capacity of each specimen. **Fig. 42** shows the test setup for the loading phase. The specimen was fixed at the top flange using threaded rods and was uplifted with a steel plate positioned beneath the specimen. By fixing at the top flange, it was able to detach the concrete surface at the bottom flange, inducing cantilever behavior during loading. At the bottom flange, a manual actuator was mounted on a cylinder load plate with a load cell attached to the opposite face. Anchor chucks locked the prestressing strand in position. During the loading experiment, hydraulic pumps applied forces to the specimen through a manual actuator. The actuator stroke was locked by anchor chucks at both ends, returning loads through the load plate.

Fig. 42 Test setup for loading specimens

Fig. 43 shows the cracking pattern observed in each specimen after either reaching a displacement of 0.5 in. or when the cracks elongated from the top surface to the bottom surface. In a steel specimen, four cracks appeared throughout the web region, with two major cracks elongating above the steel plate. The maximum crack length was 9 in. with a crack width of 0.02 in. In SMA-1 and SMA-2 specimens, a single crack appeared near the steel plate. In the steel specimen, the transverse steel stirrups have ribs that redistribute the stresses after initial cracking. In contrast, the SMA specimens were composed of plain SMA stirrups, which cannot redistribute stress. The cracking load measured by the load cell was 2.7 kips, 5.0 kips, and 4.0 kips in the steel specimen, the SMA-1 specimen, and the SMA-2 specimen, respectively. Although there was no redistribution of stresses, the prestressing effect by transverse SMA reinforcements increased the initial cracking load (85% in SMA-1 and 48% in SMA-2 specimens), which is desirable for mitigating splitting cracks during the prestress release.
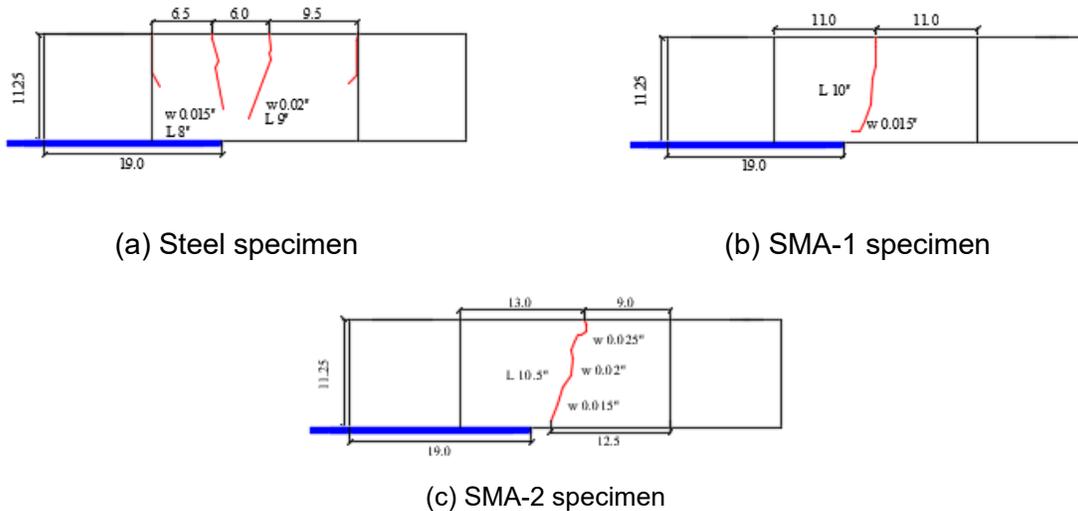
(a) Steel specimen

(b) SMA-1 specimen

(c) SMA-2 specimen

Fig. 43 Loading test results (unit: in.)

The experimental results were verified theoretically as shown in **Fig. 44** and **Eqs. (3)** to **(5)**. **Fig. 44(a)** shows schematically the load and reaction force applied at the girder, and **Fig. 44(b)** shows the resulting bending moment diagram. Based on the bending moment diagram, it was assumed that the cracking moment is 22.6 times the applied load with a given specimen condition. Using the analysis of the bending moment, section analysis was performed for each specimen to estimate the cracking moment. The compressive strength of each specimen was measured as 10.9 ksi, 9.9 ksi, and 10.3 ksi, in steel, SMA-1, and SMA-2 specimens, respectively, by cylinder compression test. According to ACI 318-19 (ACI 318 2019), the tensile strength of each specimen was decided as 0.78 ksi, 0.75 ksi, and 0.76 ksi. **Eq. (3)** shows the calculation process of theoretical cracking load, where M_{cr} is cracking moment (kips-in.), f_r is tensile strength of concrete (ksi), I_g is inertia moment (in.^{4}), y is distance from section centroid to bottom fiber (in.), σ_{SMA} is compressive stress measured at the top fiber of concrete (ksi), and P_{cr} is cracking load (kips). The experimental and theoretical results showed differences of 8.3%, 4%, and 0%, respectively, proving the accuracy of the theoretical interpretation. Additionally, replacing two steel stirrups at the further end increased cracking capacity by 85% even without the third steel stirrup layer. SMA stirrups have proven their effectiveness for mitigating end splitting cracks during prestress release.

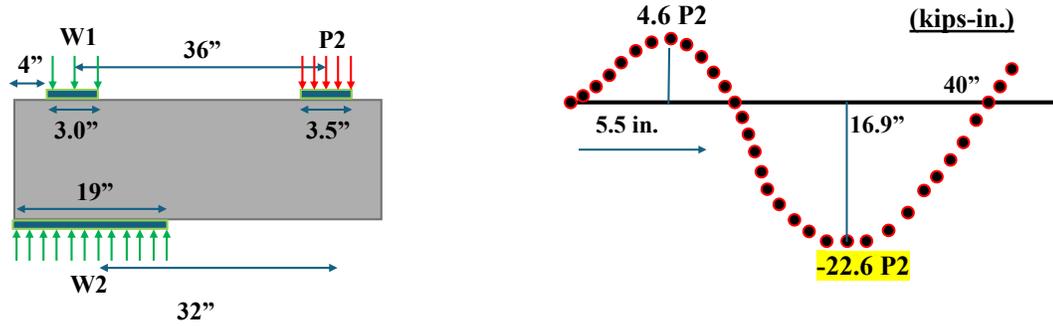$$M_{cr} = \frac{f_r I_g}{y} = \frac{0.78 \times 474.6}{5.625} = 66.1 \text{ (kips-in)}$$

$$P_{cr} = \frac{M_{cr}}{22.6} = 2.9 \text{ (kips)}$$

(3)

$$M_{cr} = \frac{(f_r + \sigma_{SMA})I_g}{y} = \frac{(0.75 + 0.65) \times 474.6}{5.625} = 117.6 \text{ (kips-in)}$$ (4)

$$P_{cr} = \frac{M_{cr}}{22.6} = 5.2 \text{ (kips)}$$

$$M_{cr} = \frac{(f_r + \sigma_{SMA})I_g}{y} = \frac{(0.76 + 0.32) \times 474.6}{5.625} = 91.1 \text{ (kips-in)}$$ (4)

$$P_{cr} = \frac{M_{cr}}{22.6} = 4.0 \text{ (kips)}$$

| (a) Load and reaction force | (b) Beam moment diagram |

Fig. 44 Theoretical approach for calculating cracking load

5.8 Healing of damaged precast girder

Fig. 45 shows the manufactured specimen mold and the figure after pouring the concrete. The basic shape of the specimen was identical to the specimen made in section 5.7. The only difference was that the SMA bars were bent 90 degrees at the tip, without crimping sleeves to the SMA bars. Additionally, a single SMA bar replaced the steel stirrup at the far end.

| (a) Specimen mold | (b) Concrete pouring and casting |

Fig. 45 Specimen manufacturing process

After casting the concrete, the specimen was loaded to induce a splitting crack in the web region. **Fig. 46** shows the cracking pattern at the web region by concentric loading. In the front face, the cracking elongated 8.5 in. with a maximum crack width of 0.025 in. At the rear face, the cracking extended to 9 in. with a maximum crack width of 0.02 in. The cracking load was measured as 1.7 kips when the first crack appeared. A single crack occurred near the steel plate under concentric loading. The strain value at the web before cracking was measured as 221 $\mu\varepsilon$. Without introducing SMA prestressing force, the cracking capacity of the specimen was reduced compared to the experiments conducted in section 5.7.

(a) Front face of the specimen   (b) Cracking at the rear face

**Fig. 45** Specimen cracking by loading

After conducting a load test, the SMA bars were heated in the test setup shown in **Fig. 46**. Induction heating was used to activate the SMA bars and heal the specimen. By SMA activation, the average compressive strain achieved at the first layer of concrete strain gauges was 78.7 $\mu\varepsilon$. Consequently, the crack width decreased to 0.005 in., representing 25% of the original crack width (75% crack width reduction). Although the crack was not fully closed, a single layer of SMA has proven its effectiveness in healing the structure.
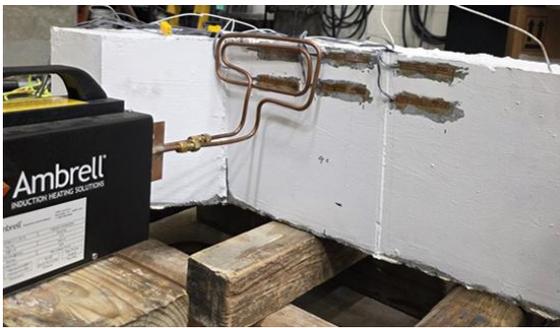
(a) SMA activation view at side face   (b) SMA activation view at top face
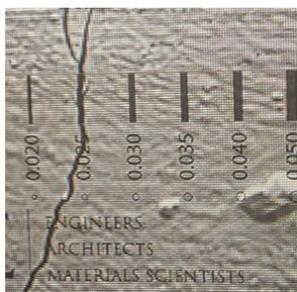
(c) Before healing   (d) After healing

Fig. 46 SMA activation test setup and experiment results

6. Conclusions and recommendations:

This project introduced an innovative method that uses SMA as transverse reinforcement in the end region of precast prestressed girders. Damage mitigation during prestress release of a prestressed concrete girder was numerically and experimentally studied by placing transverse SMA bars inside the concrete at the end region of the girder and generating the prestressing force

by SMA activation. The internal use of the NiTiNb bar was experimentally and numerically explored by examining the SMA's opening behavior during activation and the SMA bar's opening into the concrete. The numerical modeling technique was developed based on the experimental results, and parametric studies were conducted. The increased capacity of the prestressed precast concrete girder due to excessive prestressing force was experimentally investigated by manufacturing a reduced-scale girder specimen and applying concentric forces to propagate cracks in the girder's web. The healing effect of SMA activation was also explored to verify the transverse SMA's effectiveness in damaged girder conditions. Based on the results, the following conclusions were drawn:

1. In the finite element analysis on the BT-72 precast prestressed girder, using SMA stirrups proved their effectiveness in mitigating splitting cracks at the web region. The crack area was reduced by up to 25.5%, resulting in the crack width falling within an acceptable range for deicing chemicals not to penetrate. Using the transverse prestressing effect of the SMA stirrup also made it possible to reduce the number of end stirrups from five to three, while still decreasing damage in the end region.

2. The feasibility of SMA reinforcement in the end regions was shown in the finite element analysis of an AASHTO Type III prestressed girder model by evaluating the structure's performance during prestress release and loading phases. The splitting cracks were mitigated by using SMA stirrups in the prestress release phase, and the shear performance was similar to that of the ordinary steel reinforced model.

3. The numerical modeling method of SMA bar behavior during SMA activation was successfully performed by simulating the bending process and activation process through assigning different strain values at the divided section of the bent region. The accuracy of finite element analysis results was 92% and 100%, respectively, when compared with the experimental results from the non-strained and pre-strained specimens.

4. Throughout the experimental and numerical studies of SMA bars' influence on concrete during activation, sufficient clear cover (i.e., 1.0 in.) of concrete at the bar opening location was found to be necessary in using SMA bars internally.

5. By an appropriate bonding method of the SMA bar to concrete (i.e., bending the end tips, attaching sleeves on the surface of the bar), the recovery stress built by SMA activation was fully transferred to the concrete as a prestressing force.

6. The prestressing vertical force applied by SMA transverse reinforcements during activation was evaluated to increase the crack resistance in the de-tensioning stage of prestressed concrete. Using two SMA stirrups in the end region increased the cracking load by 85%.

7. SMA transverse reinforcements were useful in healing the precast concrete girder, with the crack width decreasing by 75% after activating a single SMA bar.

7. <u>Practical application/impact on transportation infrastructure:</u>

This research proposed an innovative, yet practical solution to the long-standing problem of end-region damages in PC bridge girders due to prestressing application. The project proposed a new application of an emerging class of smart materials, i.e., SMAs, as internal reinforcement in precast concrete. SMA transverse reinforcement, with its shape recovery capability, can prevent end-region cracking while reducing steel congestion at these highly-reinforced regions in bridge

girders. The results of this University Transportation Center (UTC) project will directly impact transportation infrastructure by improving serviceability, structural safety, constructability, and long-term maintenance. The longevity and durability of PC bridges will be enhanced by strengthening the end region using a unique prestressing reinforcement (SMA) that can be prestressed using heat. The transversely reinforced SMA bars will offer a cost-effective novel solution by applying prestressing forces at the crack-closing (transverse) direction, thereby preventing splitting cracks during the prestress release. The large amount of steel reinforcement that is typically required at the end region to mitigate damage at the girder's end region will also be reduced by introducing the thermally-stressed SMA bars. Increased crack resistance from the vertical prestressing force will allow larger spacing and the use of smaller-diameter reinforcements, which will, in turn, improve the constructability of larger PC bridge girders.

8. **References:**

AASHTO. 2024. *AASHTO LRFD Bridge Design Specification*. 10th edition. Washington, DC: American Association of State Highway and Transportation Officials.

Abaqus, G. 2025. "Abaqus 6.25." *Simulia Corporation*, Dassault Systems.

ACI 318. 2019. *Building Code Requirements for Structural Concrete and Commentary*. American Concrete Institute.

ACI Committee 224. 2001. *Control of Cracking in Concrete Structures*. Farminton Hills, MI: American Concrete Institute.

Andrawes, B., M. Sung, and S. Park. 2024. "NiTiNb Shape Memory Bars for Concrete Prestressing Applications." SSRN.

Breen, J. 1994. *Anchorage zone reinforcement for post-tensioned concrete girders*. Transportation Research Board.

Caro, L. A., J. R. Martí-Vargas, and P. Serna. 2013. "Prestress losses evaluation in prestressed concrete prismatic specimens." *Engineering Structures*, 48: 704–715. https://doi.org/10.1016/j.engstruct.2012.11.038.

Chen, Q., and B. Andrawes. 2017. "Cyclic Stress–Strain Behavior of Concrete Confined with NiTiNb-Shape Memory Alloy Spirals." *Journal of Structural Engineering*, 143 (5): 04017008. https://doi.org/10.1061/(ASCE)ST.1943-541X.0001728.

Choi, E., Y.-S. Chung, Y.-W. Kim, and J.-W. Kim. 2011. "Monotonic and cyclic bond behavior of confined concrete using NiTiNb SMA wires." *Smart Materials and Structures*, 20 (7): 075016. https://doi.org/10.1088/0964-1726/20/7/075016.

Dagdelen, F., E. Balci, I. N. Qader, E. Ozen, M. Kok, M. S. Kanca, S. S. Abdullah, and S. S. Mohammed. 2020. "Influence of the Nb Content on the Microstructure and Phase Transformation Properties of NiTiNb Shape Memory Alloys." *JOM*, 72 (4): 1664–1672. https://doi.org/10.1007/s11837-020-04026-6.

Dommer, K., and B. Andrawes. 2012. "Thermomechanical Characterization of NiTiNb Shape Memory Alloy for Concrete Active Confinement Applications." *Journal of Materials in Civil Engineering*, 24 (10): 1274–1282. https://doi.org/10.1061/(ASCE)MT.1943-5533.0000495.

Dunkman, D. A. 2009. "Bursting and Spalling in Pretensioned U-Beams."

Fenwick, R. C., and S. C. Lee. 1986. "Anchorage zones in prestressed concrete members." *Magazine of Concrete Research*, 38 (135): 77–89. https://doi.org/10.1680/macr.1986.38.135.77.

Geren, K. L., and M. K. Tadros. 1994. "The NU Precast/Prestressed Concrete Bridge I-Girder Series." *PCI journal*, 39 (3): 26–39.

Gergely, P., and M. A. Sozen. 1967. "Design of Anchorage-Zone Reinforcement in Prestressed Concrete Beams." *PCI Journal*, 12 (2): 63–75. https://doi.org/10.15554/pcij.04011967.63.75.

Ghafoori, E., M. Neuenschwander, M. Shahverdi, C. Czaderski, and M. Fontana. 2019. "Elevated temperature behavior of an iron-based shape memory alloy used for prestressed strengthening of civil structures." *Construction and Building Materials*, 211: 437–452. https://doi.org/10.1016/j.conbuildmat.2019.03.098.

Hognestad, E. 1951. "Study of combined bending and axial load in reinforced concrete members." *University of Illinois. Engineering Experiment Station. Bulletin; no. 399*.

Ibell, T. J., and C. J. Burgoyne. 1993. "Experimental investigation of behaviour of anchorage zones." *Magazine of Concrete Research*, 45 (165): 281–291. https://doi.org/10.1680/macr.1993.45.165.281.

Iyengar, K. T. S. R., and M. K. Prabhakara. 1971. "Anchor Zone Stresses in Prestressed Concrete Beams." *Journal of the Structural Division*, 97 (3): 807–824. https://doi.org/10.1061/JSDEAG.0002846.

Jiang, S., Y. Liang, Y. Zhang, Y. Zhao, and C. Zhao. 2016. "Influence of Addition of Nb on Phase Transformation, Microstructure and Mechanical Properties of Equiatomic NiTi SMA." *Journal of Materials Engineering and Performance*, 25 (10): 4341–4351. https://doi.org/10.1007/s11665-016-2281-3.

Jung, D., J. Wilcoski, and B. Andrawes. 2018. "Bidirectional shake table testing of RC columns retrofitted and repaired with shape memory alloy spirals." *Engineering Structures*, 160: 171–185. https://doi.org/10.1016/j.engstruct.2017.12.046.

Liao, L., A. De La Fuente, S. Cavalaro, A. Aguado, and G. Carbonari. 2015. "Experimental and analytical study of concrete blocks subjected to concentrated loads with an application to TBM-constructed tunnels." *Tunnelling and Underground Space Technology*, 49: 295–306. https://doi.org/10.1016/j.tust.2015.04.020.

Marshall, W. T., and A. H. Mattock. 1962. "Control of Horizontal Cracking in the Ends of Pretensioned Prestressed Concrete Girders." *PCI Journal*, 7 (5): 56–74. https://doi.org/10.15554/pcij.10011962.56.74.

McCormick, N., and J. Lord. 2010. *Digital image correlation*. 52–54. Materials Today.

O'Callaghan, M. R., and O. Bayrak. 2007. "TENSILE STRESSES IN THE END REGIONS OF PRETENSIONED I-BEAMS AT RELEASE." *Electronic thesis. Univ. of Texas at Austin*.

Pan, S., D. Yan, X. Zhang, C. Zou, Y. Chen, H. Hui, S. Chen, and B. Andrawes. 2023. "Investigation on recovery stress and stability of hot-drawn $Ni_{47} Ti_{44} Nb_9$ SMA." *Smart Materials and Structures*, 32 (3): 035041. https://doi.org/10.1088/1361-665X/acbbfe.

Park, S., and B. Andrawes. 2025. "Application of NiTiNb shape memory alloys in the end region of prestressed concrete bridge girders." *Advances in Structural Engineering*, 13694332251340717. https://doi.org/10.1177/13694332251340717.

PCI. 2023. *PCI Bridge Design Manual, 4th Edition*. 4th ed. Precast/Prestressed Concrete Institute.

Pérez-Claros, E., and B. Andrawes. 2025. "Experimental Testing of Concrete Crossties Prestressed with Shape Memory Alloys." *Journal of Transportation Engineering, Part A: Systems*, 151 (10): 04025073. https://doi.org/10.1061/JTEPBS.TEENG-8982.

Ronanki, V. S., D. I. Burkhalter, S. Aaleti, W. Song, and J. A. Richardson. 2017. "Experimental and analytical investigation of end zone cracking in BT-78 girders." *Engineering Structures*, 151: 503–517. https://doi.org/10.1016/j.engstruct.2017.08.014.

Ross, B. E., M. D. Willis, H. R. Hamilton, and G. R. Consolazio. 2014. "Comparison of details for controlling end-region cracks in precast, pretensioned concrete I-girders." *PCI Journal*, 59 (2): 96–108. https://doi.org/10.15554/pcij.03012014.96.108.

Sarles, D., and R. Y. Itani. 1984. "Effect of End Blocks on Anchorage Zone Stresses in Prestressed Concrete Girders." *PCI Journal*, 29 (6): 100–114. https://doi.org/10.15554/pcij.11011984.100.114.

Sherif, M., O. Ozbulut, A. Landa, and R. F. Hamilton. 2014. "Self-Post-Tensioning for Concrete Beams Using Shape Memory Alloys." In: *Volume 2: Mechanics and Behavior of Active*

Materials; Integrated System Design and Implementation; Bioinspired Smart Materials and Systems; Energy Harvesting, V002T04A014. Newport, Rhode Island, USA: American Society of Mechanical Engineers.

Shin, M., and B. Andrawes. 2010. "Experimental investigation of actively confined concrete using shape memory alloys." *Engineering Structures*, 32 (3): 656–664. https://doi.org/10.1016/j.engstruct.2009.11.012.

Shin, M., and H. Yu. 2018. "A Parametric Study on the Splitting/Bursting Damage of Prestressed Concrete Prisms." *Sci. age Exp.*

Steensels, R., B. Vandoren, L. Vandewalle, and H. Degée. 2019. "Evaluation of end-zone detailing of pre-tensioned concrete girders." *Engineering Structures*, 187: 372–383. https://doi.org/10.1016/j.engstruct.2019.02.068.

Suhail, R., G. Amato, and D. P. McCrum. 2020. "Active and passive confinement of shape modified low strength concrete columns using SMA and FRP systems." *Composite Structures*, 251: 112649. https://doi.org/10.1016/j.compstruct.2020.112649.

Sung, M., and B. Andrawes. 2024. "Innovative precast prestressed concrete truss system using shape memory alloys and conventional steel." *Journal of Intelligent Material Systems and Structures*, 35 (10): 875–891. https://doi.org/10.1177/1045389X241239701.

Trabucchi, I., G. Tiberti, A. Conforti, F. Medeghini, and G. A. Plizzari. 2021. "Experimental study on Steel Fiber Reinforced Concrete and Reinforced Concrete elements under concentrated loads." *Construction and Building Materials*, 307: 124834. https://doi.org/10.1016/j.conbuildmat.2021.124834.

Zhao, H., and B. Andrawes. 2020. "Local strengthening and repair of concrete bridge girders using shape memory alloy precast prestressing plate." *Journal of Intelligent Material Systems and Structures*, 31 (11): 1343–1357. https://doi.org/10.1177/1045389X20916793.

9. Acknowledgements